Predicted and observed settlements induced by the mechanized tunnel excavation of metro line C near S. Giovanni station in Rome

Salvatore Miliziano [a], Armando de Lillis [a,*]

[a] *Department of Structural and Geotechnical Engineering, Sapienza University of Rome, via Eudossiana 18, 00184 Rome, Italy*

[*] *corresponding author: armando.delillis@uniroma1.it*

Abstract

This paper deals with the effects induced by the mechanized excavation of Rome metro line C in the area of an old masonry building, the Carducci school. Class A settlements predictions are obtained performing full 3D soil-tunnel-structure interaction numerical analyses, using a simple elastic perfectly plastic soil constitutive model. The developed model realistically simulates the main excavation and construction features influencing the induced settlements, such as tunnel advancement, front pressure, TBM-EPB design (shield's weight, overcut and conicity), tail void grouting and grout hardening over time. The measured settlements are reported and compared with the results of numerical analyses performed before (class A prediction) and after tunnelling; the latter carried out to implement in the model the front pressure and TBM conicity actual values, both higher than assumed in the design. Since before the excavation the foundations were reinforced with micropiles, and these were not modelled, the comparison between monitoring data and numerical predictions is limited to the settlements outside the building. Monitoring data are also compared with further analyses conducted using small-strain soil stiffness and using a constitutive model able to reproduce the non-linearity of soil behavior (Hardening Soil). The different predictions of the two models are investigated analyzing the vertical strains distributions and the stress paths around the tunnel. Finally, a reasonable interpretation for the remaining differences between numerical results and field data is proposed and used to back-analyze the settlements, obtaining a satisfactory agreement. The results confirm the effectiveness of the proposed 3D numerical approach, associated with relatively simple

soil constitutive models, as a tool to predict tunnelling-induced settlements both in the design and the construction phase, independently of the geotechnical context.

Keywords: mechanized tunnelling; 3D modelling; settlements; monitoring.

1. Introduction

The study of surface effects due to tunnelling in urban areas is of special interest as potential damages to interacting vulnerable buildings and protective measures must be identified and quantified beforehand. Several approaches at different level of detail can be used to this aim. In a preliminary study, tunnelling-induced displacements can simply be assessed through Gaussian curves (Peck, 1969) and the damage to existing buildings can be evaluated assuming that greenfield displacements will apply directly to the structure following, for instance, the approaches proposed by Burland (1995) or by Boscardin and Cording (1989). At a further stage, the soil-tunnel-existing buildings interaction can be modeled two dimensionally (2D) introducing various simplifications to take into account both the three-dimensionality of the excavation process (Rowe and Kack, 1983; Negro and De Queiroz, 2000; Tamagnini et al., 2005; Altamura et al., 2007; Möller and Vermeer, 2008) and of the building structures (Miliziano et al., 2002). These approaches drastically simplify the real problem and, moreover, assumptions about the volume of the subsidence basin - based on instances in similar tunnels, excavated with similar machines, driven similarly in similar geotechnical contexts - are required in advance.

A more rigorous approach consists in performing three-dimensional (3D) numerical analyses, which allow to simulate explicitly: *i*) the main features of the excavation; with specific reference to mechanized tunnel excavation, since the first comprehensive numerical modelling attempt (Lee and Rowe, 1991), considerable progress has been made (Swoboda and Abu-Krisha, 1999; Kasper and Meschke, 2004; Logarzo et al., 2011; Lambrughi et al., 2012; Kavvadas et al., 2017; de Lillis et al., 2018; Ochmański et al., 2018, Zhou et al., 2018); *ii*) the soil-tunnel-existing building interaction either using an equivalent solid (Pickhaver et al., 2010; Maleki et al., 2011, Farrell et al., 2014, Losacco et al., 2014; Bilotta et al., 2017) or a detailed structural model (Burd et al., 2000; Giardina et al., 2010;

Fargnoli et al., 2015a; Fargnoli et al., 2015b; Giardina et al., 2015; Franza et al., 2017). It is worth noting that by adopting a fully 3D numerical approach and simulating explicitly the main factors influencing the surface effects, the settlements profile and the volume of the subsidence basin are analysis results and not mere assumptions as occurs with simplified approaches. Clearly the most satisfactory approach, 3D modelling is also increasingly manageable thanks to the development of reliable commercial numerical codes and to the advances in computational power.

This paper deals with the interaction between the mechanized tunnel excavation of Rome metro line C and an old masonry building, the Carducci school, located near the existing S. Giovanni metro A station. A fully 3D finite element numerical model was developed including the main features of the tunnel excavation and construction processes influencing the surface settlements, such as front pressure, geometry (including cutterhead overcut and conicity) and weight of the shield, tail void grouting and grout hardening over time. A simplified but realistic simulation of the masonry building, accounting for both its stiffness and weight, was also implemented in the model.

Preliminary analyses and class A numerical predictions were published prior to the start of the excavation (Formato, 2009; Buselli et al., 2011). Upon completion of the tunnel, monitoring data were compared with the results of further analyses, carried out to update the prediction according to two constructional changes: the actual TBM conicity and the earth pressure in the excavation chamber were in fact both appreciably higher than originally assumed in the design. Despite the Class A analysis showed that no appreciable tunnelling-induced damage was expected on the building, before the excavation the foundations were reinforced with micropiles (not included in the numerical model). Therefore, the comparison was limited between settlements field data recorded outside the building, where the effects of the micropiles are expected to be negligible, and greenfield numerical results. The measured settlements were then compared with two additional numerical analyses, performed to investigate the influence of soil stiffness and soil constitutive model. In boundary value problems where a good prediction of the effects induced on pre-existing structures is needed, in fact, the use of constitutive models able to well simulate the non-linear soil behaviour in the range of small-to-medium strain levels, can be essential (Rotisciani and Miliziano, 2014; Rotisciani et al., 2015). A final analysis was carried out to back-analyze the differences between monitoring data and numerical results on the basis of a reasonable physical interpretation.

The results confirm the effectiveness and reliability of the proposed numerical approach, associated with relatively simple soil constitutive models, to predict tunnelling-induced settlements and damages independently of the geotechnical context.

2. Tunnels and building

The construction of Rome metro line C involved the excavation of two single-track tunnels (tunnels A and B). The tunnels were realized using two TBMs equipped with EPB technology. The excavation diameter is 6.70 m, the shield diameter (*D*) is 6.69 m. The lining ring consists of seven 0.30 m thick pre-cast reinforced concrete elements and its external diameter is 6.4 m. Thus, the annulus between the lining and the excavation profile is 0.15 m thick. The shield is slightly conical, the tail diameter is 30 mm smaller than the excavation diameter (20 mm conicity + 10 mm cutterhead overcut).

The tunnels lie beneath the city center, where several buildings of historical and social interest are located; among the most important structures, the Carducci school is placed between 7.2 m and 9.3 m from the tunnel B axis (tunnel A is 23 m away). The main southeast façade of the building is almost parallel to the axis of the tunnels. Near the building, the TBMs operated just beneath the water table with a soil cover of about 22 m. Fig. 1 shows a plan view of the building and the tunnels. The building is about 15 m high and the ground plan is almost rectangular (Fig. 2). The structure is composed of two parts: the main original body, built in 1912 along via La Spezia, and the extensions added at both ends in the 1940's. Fig. 3 reports the building ground plan of the oldest part. The building was constructed using "Roman masonry", that is bricks alternating with tuff. The foundation of the original building is continuous on isolated masonry piers, which are based approximately 10 m below the ground surface. The foundation of the extensions is a shallow reinforced concrete slab 4.5 m below the ground surface. Some damages and a large number of cracks were detected on the building before tunnelling.

3. Soil profile, pore pressure regime and physical-mechanical soil parameters

Soil profile and hydraulic conditions were determined through an extensive geotechnical investigation, involving laboratory and *in-situ* tests, thoroughly described in Formato (2009). The building is located close to the "Marana of Acqua Mariana", an ancient ditch that completely eroded the volcanic sediments; thus, the hard pyroclastic layers commonly found in the area are absent immediately beneath the building. The engraved area of the ditch was subsequently filled by fluvial-alluvial deposits (geological map in Fig. 4, adapted from Ventriglia, 2002). The underlying fluvial pre-volcanic deposit is composed of three main slightly over-consolidated levels (OCR = 2). A thick layer of man-made ground covers all the natural formations. From the ground surface (37 m amsl) the following layers are encountered:

- man-made ground (**R**): medium dense to loose coarse-grained soil, including relicts of ancient structures; the thickness of this layer is approximately 16 m at the building site;
- recent fluvial-alluvial deposit (**LSO**): clayey silt and sandy silt, locally reaches a maximum thickness of 18 m;
- pre-volcanic fluvial deposit: very dense silty sand and clayey silt **(St)**, clayey silt and silty clay **(Ar**) and sandy gravel **(Sg**).

At the bottom of the Pleistocenic fluvial deposit, the bedrock consists of hundreds of meters of stiff overconsolidated Pliocenic clay, **Apl**. The geotechnical cross-section is represented in Fig. 5.

Based on piezometric measurements, the pore pressure distribution in the man-made ground and in the **Sg** sandy gravel layer is hydrostatic, with piezometric surfaces located at 28 m amsl and 18 m amsl, respectively. The measured pore pressure distribution in the clayey strata (**LSO**, **St**, **Ar**) varies according to a downward one-dimensional steady-state flow.

The main results of the geotechnical investigation are reported in Fig. 6. Young's moduli appropriate for medium-large deformation levels, E, were determined from SPT and CPT *in-situ* tests using empirical correlations (Denver, 1982; Robertson and Campanella, 1983) and interpreting pressuremeter test results (Menard, 1976; Mair and Wood, 1987). Small-strain Young's moduli, E_0, were obtained from cross-hole tests. The horizontal effective stresses are calculated according to Mayne and Kulhawy's equation (1982) for the coefficient of earth pressure at rest, $K_0 = (1 - \sin\varphi')\cdot OCR^{\sin\varphi'}$, and all layers are characterized by a Poisson's ratio, ν, equal to 0.3. The soil is modelled as an elastic perfectly plastic material with a Mohr-Coulomb strength criterion. The physical and mechanical soil parameters are summarized in Table 1; for each lithotype, Young's moduli increase with depth in the reported ranges.

4. Numerical model

The numerical model was set up using the finite element commercial code Plaxis 3D Tunnel (2007). The model is 140 m wide, 45 m deep, and the length in the tunnel direction is 225 m (Fig. 7). To minimize the influence of the boundaries, according to Franzius and Potts (2005), the longitudinal distances to the remote vertical boundaries are 7*D* and 13*D*, in front of and behind the building, respectively. In the longitudinal direction the mesh is divided in 2.5 m thick slices. Horizontal restraints are applied to all the vertical boundaries, while both horizontal and vertical displacements are restrained at the bottom boundary. The analyses do not extend into the deeper stiff layer **Apl**. The adopted mesh is coarse (Fig. 7), with local refinements around the tunnel. 15-node wedge finite elements with second order interpolation for displacements are adopted and the integration involves six stress points.

The TBM has a 6.7 m diameter and the shield, 10 m long, is modeled using ring plate elements weighing 56 kN/m, which represents the full weight per meter of the machine, including all the equipment. The construction process is simulated discontinuously (step by step), removing 2.5 m thick slices of elements inside the excavation profile for each step while, at the same time, the TBM shield advances, activating plate elements at the front and deactivating them behind the tail. To reproduce both the cutterhead overcut and the conicity of the shield, the diameter of the ring plate employed to simulate the shield is gradually reduced from 6.70 m at the front to 6.68 m at the tail. The sum of TBM conicity and cutterhead overcut at the time of the design, in fact, was supposed to be only 20 mm, 10 mm less than the actual value (30 mm). The lining is simulated as continuous and homogeneous using shell elements with a 6.4 m external diameter, switched on behind the shield's tail. Both the TBM and the tunnel lining are modeled as linear elastic; Young's moduli, Poisson coefficients, flexural stiffnesses, *EI*, and normal stiffnesses, *EA*, are listed in Table 2.

The distribution of the front pressure was originally assumed equal to the active total horizontal pressure, according to the design front pressure distribution, namely 150 kPa at the crown linearly increasing toward the invert (12 kPa/m).

The backfilling of the tail void can be simulated through the application of a distributed pressure acting normally to the soil surrounding the annular gap (for instance Zhang et al., 2016). A more accurate modelling of the tail void grouting can be achieved by means of continuum elements whose mechanical properties can be modified progressively according to the hardening of the grout (Lambrughi et al., 2012, Shah et al., 2018). Hence, behind the TBM, continuum linear elastics elements are activated to fill the tail void (15 cm thick) and the grout injection pressure is simulated applying an axial stress in the opposite direction of the tunnel advancement to the ring cluster between the lining and the surrounding soil, 50 kPa higher than the maximum value of the front pressure. The grout is assumed to be hardened after 10 m: fresh grout is incompressible and has a low shear modulus (γ = 21 kN/m^3, E = 1 MPa, ν = 0.49) while hard grout is very stiff (E = 14 GPa, ν = 0.15).

Since preliminary simplified calculations showed that the settlements induced by the furthest tunnel (tunnel A) on the building are negligible, only the excavation of tunnel B is simulated. The main features of the excavation simulation are schematically summarized in Fig. 8.

The building is modelled quite realistically, taking into account both its stiffness and weight. The main part of the building is simulated modelling the load bearing and gable walls (Fig. 9) using elastic perfectly plastic continuum elements with a Mohr-Coulomb strength envelope and a tension cut-off. Selected stiffness and strength parameters (E = 1.3 GPa, c = 280 kPa, φ = 40° and tensile strength, σ_t, equal to 60 kPa) are appropriate for Roman brickwork. The floor slabs are not modelled explicitly but their weight and surcharges are simulated applying an equivalent uniform load (15 kPa for each floor) on the bearing walls. Because of the large distance from the tunnels, only the concrete slab foundation of the new part of the building is modelled; the weight of the building is taken into account trough a distributed load of 10 kPa for each floor. The foundations are simulated using elastic continuum elements with a Young's Modulus of 31 GPa and a Poisson's ratio of 0.15. Soil and structure interact through a purely frictional interface, whose friction angle is assumed equal to 0.7 times that of the surrounding soil.

Due to the relatively small thickness of the **LSO** layer around tunnel B (see Fig. 5) and the high permeability of the other layers, all analyses were performed assuming drained conditions.

5. Class A numerical prediction

5.1 Preliminary analyses

To achieve a reasonable compromise between accuracy of results and calculation time in both greenfield and interaction analyses, the influence of mesh density and tolerated error was studied using a relatively small portion of the entire mesh (the longitudinal length was reduced from 225 m to 60 m).

Fig. 10 shows the vertical displacement at ground level above the tunnel crown, w_c, normalized to the maximum calculated value, w_{max}, and the calculation times obtained using several mesh densities and tolerated errors. The accuracy of the solution and the calculation time raise as the mesh density is increased and the tolerated error is decreased. A time/accuracy compromise deemed acceptable is achieved using a coarse mesh (6 800 elements with average dimension of about 1 m) and a tolerated error of 0.01. The difference between this solution and the most accurate one, obtained adopting a very fine mesh (37 145 elements with average size of 0.40 m) and a 0.001 tolerated error, is about 3% with respect to settlements and the calculation time is roughly 1/20.

Using the entire mesh, another preliminary analysis was carried out in greenfield condition to assess boundary effects on the numerical solution and confirm the adequacy of the longitudinal length. Fig. 11 shows the numerical subsidence trough’s volume normalized to the nominal excavation volume (volume loss, V_L), along cross section 2 (see Fig. 3). Settlements induced by tunnelling are inappreciable ($V_L = 0$) until the excavation front reaches a distance of about 7*D* (47 m) from the reference section; then V_L regularly increases as the excavation front advances and reaches a maximum value of about 0.75% 5*D* beyond the considered section. Further advancements of the excavation do not affect the value of V_L; thus, the 33*D* mesh length can be considered adequate.

5.2 Soil-tunnel-existing building interaction analysis

Full interaction analyses were carried out to study the interaction between soil, tunnel and existing building. Before the simulation of the excavation, the building was implemented in the model and the induced displacements were then set equal to zero, in order to isolate the effects induced by tunnelling. The application of the building self-weight did not produce any damage to the structure. The effects of the building presence on the settlements are apparent in Fig. 12 and Fig. 13, where the settlements calculated at the foundation level (-4.5 m) during and at the end of the excavation along sections 1 and 2 (see Fig. 3) respectively, are reported. Along section 1, the maximum value of the settlements is in the 6-7 mm range and, due to the small amount of plastic deformation developed (Formato, 2009), the settlement just above the front is about 1/3 of the final settlement, as expected when the soil behavior is substantially elastic (Panet and Guenot, 1982). The building's presence has a small influence on the longitudinal settlements curves; underneath the structure the settlements are slightly bigger than those obtained in greenfield conditions and during the advancement of the excavation the response is barely stiffer. Along cross section 2, a relatively small increment of settlements under the building can be noted in comparison with the greenfield settlements profile, also reported in Fig. 13. Due to the stiffness of the building, however, the deflection ratio (as defined by Burland and Wroth, 1974) is 0.0014%, smaller than that calculated in greenfield conditions (0.0036%), and both are extremely small in absolute value.

The maximum settlement is about 8.5 mm and, because of the stratigraphic heterogeneity, the settlement curves appear slightly nonsymmetrical. The numerical result matches quite well the Gaussian distribution as originally proposed by Peck (1969), and successively adapted by Moh et al. (1996) to calculate settlements below the ground level. The Gaussian curve was calculated using the volume of the numerical subsidence trough and selecting a value of 0.55 for the K parameter. The calculated horizontal displacement of the building's foundation is about 2.5 mm, while the relative horizontal displacements are close to zero (no horizontal strains).

The adopted approach allows to determine stress and strain distributions in the building. To assess the induced damage both in terms of potential cracks and structural safety reduction, the tensile stress and the shear strength mobilization levels are particularly relevant. As expected, because of the small level of distortion to the structure, the severity of the stress state was practically unchanged by the construction and tunnelling-induced effects on the building were negligible (Buselli et al., 2011). The category of damage evaluated following Burland (1995) results as zero.

Despite the very low damage numerically predicted, due to the poor quality and maintenance of the masonry (the building suffered some damage and a large number of cracks were detected), before the construction of the tunnel the foundations were reinforced with micropiles down to the firm **Sg** layer. The micropiles are 160 mm in diameter, 35 m in length and their spacing is 2 m in average. Also, the micropiles were connected to the existing foundation without any preloading, hence they provide a passive kind of support.

6. Observed and recalculated settlements

6.1 Monitoring data

Earth pressures were measured by sensors placed in the excavation chamber of the TBM during each construction cycle: excavation phase and subsequent lining installation phase (Fig. 14). At some distance from the school (Fig. 14a), during the excavation the earth pressure remained roughly constant, with values ranging between 270 and 320 kPa. These decreased during the ring assembly phase at the end of the cycle, ranging from 160 to 200 kPa. Near the school (Fig. 14b), to minimize induced settlements, higher earth pressures were employed. During the excavation, pressures ranged between 300 and 350 kPa, while at the end of the lining installation ranged between 270-300 kPa. class A prediction obtained by numerical analyses and published prior to tunnelling (Buselli et al., 2011) used an average earth pressure of 150 kPa, considerably lower than that actually measured during construction, at least in the area of interest to this study.

The location of all the monitoring instruments is shown in Fig. 15. To measure road settlements, benchmarks were located on Via La Spezia along cross-sections 11 and 12. To measure both the horizontal and the vertical displacements of the building, several mini-prisms were installed. When the tunnel closer to the school was driven (tunnel B), benchmarks 4 and 5 (Fig. 16, section 11), located just above the tunnel, recorded a maximum settlement of about 4 mm. The settlements steady decrease as the distance from the tunnel axis increases; the settlement for benchmark 1B was roughly zero. Ten days later, during the passage of the second TBM (tunnel A), when the front was near section 11, the benchmarks located in this section slightly rose initially (maximum measured value of about 1 mm). Then the benchmarks started to settle. After both tunnels were driven, a maximum settlement of about 13 mm was measured along section 11, halfway between the tunnels.

Fig. 16 also shows the average earth pressure in the excavation chamber, which, as stated above, as the TBM approached the school increased from about 200 kPa to about 300 kPa. Since the excavation of tunnel A affected the settlements, it was not possible to measure the final settlements induced by tunnel B only. Hence, this value has been evaluated following the trend of measured settlements after the excavation of the second tunnel. To this aim, the settlements of the benchmark 5B after the passage of tunnel A (CD curve in Fig. 17), were first normalized with respect to the final measured settlement, w_f, then used to extrapolate the evolution of settlements induced by tunnel B only (BB' curve), assuming the two trends to be coincident.

School settlements were generally below 3 mm, rising to 6 mm near the existing S. Giovanni metro station (Fig. 18). This is related to the pressure reduction in the TBM excavation chamber. As the machine approached the station, in fact, the earth pressure was deliberately reduced to a very low average value of about 120 kPa (see Fig. 16) to avoid damaging the underground structures. The deflection ratio estimated from the measured settlements along the main façade of the building is extremely low and equal to 0.0055%; even smaller in the transverse direction. Consistently with the very small settlements and deformations induced on the building, no further cracking nor appreciable widening of the pre-existing cracks were detected upon completion of the tunnel.

Since the reinforcing micropiles were not simulated in the numerical analyses, it is appropriate to compare only measured road settlements and greenfield numerical results. Thus, all the analyses reported in the following were carried out in greenfield conditions.

6.2 Updated class A greenfield prediction (class C1 prediction)

To take into account the actual pressures, measured during the tunnel excavation, and the actual TBM geometry (conicity and overcut), two new numerical analyses were performed using the numerical model set up for class A predictions. To gain some insight into the relative influence of the two changes, they were introduced in the model sequentially. A first analysis was carried out with an average pressure of 300 kPa at the front and a pressure of 350 kPa for the tail void grouting injection, while maintaining the original TBM geometry; a second analysis was conducted simulating both the measured pressures and the actual TBM geometry (conicity + overcut = 30 mm). As the only modifications introduced in the model regard constructional details, the results obtained in the last analysis constitute an update of the class A prediction (rigorously, class C1 prediction).

The settlements induced by tunnel B at ground level, extrapolated from the measurements as discussed above, are reported in Fig.19 and compared with the numerical results. In all cases, the shapes of the numerical subsidence troughs are manifestly the same, slightly asymmetrical due to the stratigraphic heterogeneity. The maximum settlement predicted in the class A analysis (7.8 mm) overestimates by 50% the measured value (5.1 mm). Considering the actual pressures, the maximum settlement lowers to 7.2 mm but rises to 9.6 mm simulating the actual TBM geometry also, almost doubling the measured value and indicating a poor accuracy of the updated prediction.

In the case at hand, the geometry of the TBM plays a much larger role than the front and grout pressures. In fact, a difference in front pressure of 100%, from the design value of 150 kPa to the actual value of 300 kPa, decreases the volume loss by just 0.07%, while a 50% difference in TBM conicity increases the volume loss by 0.17%.

6.3 Influence of soil stiffness and soil constitutive model

To investigate the influence of both the soil stiffness and the soil constitutive model, two further analyses were conducted using:

- the linear elastic perfectly plastic model, already employed in the previous analyses, adopting small-strain stiffness values (E_0), based on cross-hole tests results, about ten times higher than those used in the class A prediction (E_0-analysis; Table 1). The main objective of this analysis was to ascertain if a very simple model, calibrated at small-strain levels, could be able to simulate the deformation field induced by a TMB designed and driven specially to minimize surface settlements;

- the Hardening Soil constitutive model for the two layers in which the excavation takes place (**LSO** and **St**) and the soil behavior is expected to be highly non-linear; elsewhere, the elastic perfectly plastic model with small-strain stiffness was used. The HS model was calibrated on cross-hole tests results assuming unloading-reloading moduli (E_{ur}) equal to E_0 (HS-analysis; Table 3); thus, the elastic stiffness is the same in the two models. The aim of this analysis was to assess the predictive capability of a constitutive model still simple to use and calibrate but able to reproduce the soil non-linearity.

The maximum settlement calculated in the HS-analysis overestimates by roughly 40% the measured value (Fig. 20). A result closer to the measurements (about 20% overestimation) was obtained in the E_0-analysis.

The deformation profile along the depth between the ground level and the crown of tunnel B at the end of the excavation is reported in Fig. 21, together with the settlements profile along the same vertical, for both E_0 and HS analyses. In the same figure, the annulus around the cavity where plastic deformations developed during the excavation in the E_0-analysis is also highlighted. Since at crown depth the settlement is roughly the same in both analyses (about 22 mm), the difference in surface settlements is associated to the higher values of vertical deformations (ε_v, negative for tensile strains) obtained near the tunnel (**LSO** layer) in the E_0-analysis. From a 16 m depth to the ground level, the deformations predicted in both analyses coincide, as expected since the constitutive model in the **R** layer is the same and the deformation fields differences around the perturbation are rather small.

The described behavior can be further understood analyzing the stress and strain paths of four points located in a transversal plane (reference section) above the crown and at springline depth, reported in Fig. 22. In the same figure, the main phases of the excavation are indicated with symbols representing different values of the distance from the excavation front, *L*.

The E_0-analysis stress paths show that the principal effective stresses of the points close to the tunnel (P_1 and P_3) progressively increase as the TBM approaches the reference section. This is due to the earth pressure applied to the front during excavation, higher than the geostatic horizontal stresses. Once the front surpasses the reference section, radial stresses rapidly decrease. At the crown the major principal effective stress, σ'_{I}, (almost vertical) drops, while the minor principal effective stress, σ'_{II}, (almost horizontal) doesn't change significantly; the trend continues after the inversion of principal stresses directions (the vertical stress becomes smaller than the horizontal one). At the springline, during the progressive reduction of σ'_{II} (horizontal), due to the arching effect σ'_{I} (vertical) increases. Already in this stage of the analysis (first 2.5 m advancement beyond the reference section), the state of stress at points P_1 and P_3 reaches the failure criterion and, after that, both principal stresses reduce according to the strength law.

During the following advancements (5-7.5-10 m) both at the crown and at the springline, the radial stresses are zero, indicating that the soil does not close onto the TBM and an open gap between soil and shield persists. Simulating the soil non-linearity, the gap does not occur, but the values of radial stresses numerically obtained in the HS-analysis are close to zero. After the tail of the TBM passes the reference section and the tail void is grouted, the principal stresses increase, the stress state leaves the strength criterion and returns in the elastic domain for both P_1 and P_3 points. Similar stress paths are observed farther from the excavation: at points P_2 and P_4 the stress paths reach the strength envelope during the second TBM advancement beyond the reference section (2.5-5 m). Adopting the HS model, the ground response is dictated by the smooth elastoplastic transition and only at point P_3 (located near the springline) failure occurs.

The evolution of the radial effective stress (σ'_{V}) versus the radial strain above the crown (point P_1), reported in Fig. 22c, highlights the effects of the HS model non-linearity, which allows the progressive accumulation of plastic deformations without failing. In the E_0-analysis, smaller elastic vertical deformations, are initially obtained; after the radial stress becomes close to zero – this occurs during the third advancement of the TBM (5-7.5 m) – mainly plastic tensile strains rapidly develop, and the deformations become greater than the ones obtained with the HS constitutive law. Once the shield advances, the tail void is grouted, the radial stress increases and small compressive vertical strains take place in both analyses. The illustrated behavior is responsible of the deformations profiles differences observed in the plastic zone above the tunnel (Fig. 21) and, ultimately, of the difference of settlements induced at ground level.

6.4 Back-analyses

The very low soil stresses around the tail of the shield resulting from the HS-analysis and the presence of a gap between soil and shield highlighted by the E_0-analysis, suggested a physical interpretation of the remaining differences between numerical results and monitoring data. The hypothesis is that the high injection pressure (350 kPa) could have allowed the tail grout to push back the soil and squeeze into the newly opened gap, covering the rear part of the machine's shield. Another reasonable consideration is that near the end of the excavation (the Carducci school is close to the metro station) the cutterhead border scrapers were wore down, thus decreasing the overcut.

The hypothesized mechanisms were both numerically simulated through a reduction of the conicity (which in the model also incorporates the cutterhead overcut) to 20 mm, tentatively assuming a 10 mm reduction; thus, two further analyses were performed using the models described in 6.3. As expected, due to a much more limited impact of the plastic deformations, the two settlement troughs are almost identical (fig. 23). Furthermore, the calculated ground settlements compare satisfactorily with the monitoring data.

Table 4 summarizes the differences and the results of all the numerical analyses.

7. Conclusions

To study the surface effects induced by mechanized tunnelling during metro line C construction in Rome and to study the interaction between soil, tunnel and an old masonry building (the Carducci school), a fully 3D finite element numerical model was developed.

The model simulates the main features of the tunnel excavation and construction processes influencing the surface settlements, such as front pressure, geometry (including cutterhead overcut and conicity) and weight of the shield, tail void grouting and grout hardening over time. A realistic simulation of the masonry building is also implemented in the model. After performing preliminary analyses on a small portion of the mesh, aimed at optimizing the overall analysis by ensuring an acceptable accuracy/time compromise and quantifying the percentage of expected numerical errors, the model was used before construction to predict tunnelling-induced settlements and damages on the building (class A prediction). The computational effort associated to the optimized numerical model was quite manageable even using an entry-level computer. As the actual front pressure and TBM conicity were both higher than assumed in the design, after the tunnel construction, the model was used to update the class A prediction (class C1 prediction). Further numerical analyses were performed *i*) to evaluate the suitability of a simple elastic perfectly plastic soil model calibrated at small-strain stiffness, to reproduce the settlement trough induced by a TMB designed and driven specially to minimize induced settlements and *ii*) to assess the predictive capability of a relatively more complex constitutive model (Hardening Soil) able to simulate the non-linearity of soil behavior and *iii*) to close the gap between monitoring data and numerical results (back-analyses).

It is worth remarking that when fully 3D numerical analyses are performed and the main factors influencing the specific boundary value problem are explicitly and appropriately simulated, the settlement profile and the volume of the subsidence basin are analysis results depending on geometry, soil properties and excavation procedures, and not mere assumptions, as occurs when simplified procedures are employed.

The comparison between numerical predictions and monitoring data and the analysis of the evolution of stress and deformation states in the soil around the tunnel enabled to draw the main conclusions reported in the following.

The numerical settlement troughs resulting from all the analyses performed are consistently similar in shape and similar to the shape of the monitoring data, thus confirming the effectiveness of the model. The authors believe this accordance to be related to the explicit simulation of the primary features of the problem.

The numerical results confirm the well-known major role played by the TBM conicity and the cutterhead overcut on the induced settlements; the front pressure influence, which was only investigated in the range between at-rest and active total horizontal stresses, is smaller but still appreciable.

A constitutive model able to reproduce the non-linearity of soil behavior (such as Hardening Soil or more advanced), which allows to simulate more realistically the evolution of stress and deformations states around the tunnel, is to be preferred, especially in cases of shield conicity and overcut higher than those investigated herein (for instance when the tunnel layout involves tight curves). A simple elastic perfectly plastic soil model, calibrated at small strain, leads to reasonably accurate prediction of settlements induced by TBMs designed and driven specially to minimize surface effects, even in poor geotechnical conditions as in the case history at hand.

Most of the above conclusions are expected to remain true in different geotechnical and structural contexts.

Finally, in the opinion of the authors, the adopted approach can be considered a useful tool to predict settlements and damage due to mechanized tunnelling, properly taking into account the most important features of the excavation and construction processes and the soil-tunnel-structure interaction, independently of the geotechnical conditions. The proposed model can be used in the design phase and fully 3D parametric analyses can also be performed to anticipate how best to design and drive the machine; furthermore, the model can be employed during construction, after calibration, to predict future performances of the excavation and if necessary adjust the pressure in the excavation chamber.

Acknowledgments

The Authors wish to thank Roma Metropolitane and Metro C for providing field data, Eng. Federica Formato for her assistance in developing the model, Eng. Antonello Di Sotto for his help in elaborating monitoring data, and finally Eng. Antonio Zechini, Roma Metropolitane technical director at the time of the construction, for the technical support and the stimulating discussions useful to develop and improve the model.

References

Altamura, G., Burghignoli, A., and Miliziano, S. 2007. Modelling of surface settlements induced by tunnel excavation using the differential stress release technique. Rivista Italiana di Geotecnica, **41**(3): 33-47.

Bilotta, E., Paolillo, A., Russo, G., and Aversa, S. 2017. Displacements induced by tunnelling under a historical building. Tunnelling and Underground Space Technology, **61**, 221-232. https://doi.org/10.1016/j.tust.2016.10.007

Boscardin, M. D., and Cording, E. J. 1989. Building response to excavation-induced settlement. Journal of Geotechnical Engineering, **115**(1): 1-21. https://doi.org/10.1061/(ASCE)0733-9410(1989)115:1(1).

Burd, H.J., Houlsby, G.T., Augarde, C.E., and Liu, G. 2000. Modelling tunnelling-induced settlement of masonry buildings. Proceedings of the Institution of Civil Engineers-Geotechnical Engineering, **143**(1): 17–29. https://doi.org/10.1680/geng.2000.143.1.17.

Burland, J.B. 1995. Assessment of risk of damage to building due to tunnelling and excavation. *In* Proceedings of the 1st International Conference on Earthquake Geotechnical Engineering, IS-Tokyo, pp. 1189-1201.

Burland, J.B., and Wroth, C.P. 1974. Settlement of buildings and associated damage. *In* Proceedings of Conference on Settlement of Structures. Pentech Press, Cambridge, pp. 611-654.

Buselli, F., Formato, F., Logarzo, A., Miliziano, S., Simonacci, G., and Zechini, A. 2011. Prediction of the effects induced by the Metro C construction on an old masonry building. *In* Proceedings of the 7th International Symposium on Geotechnical Aspects of Underground Construction in Soft Ground, Rome, 2011. Balkema, Rotterdam, pp. 971-978.

de Lillis, A., De Gori, V., and Miliziano, S. 2018. Numerical modelling strategy to accurately assess lining stresses in mechanized tunneling. *In* Proceedings of the 9th European Conference on Numerical Methods in Geotechnical Engineering, Porto, 2018. CRC Press, London, pp. 1295-1302.

Denver, H. 1982. Modulus of elasticity for sand determined by SPT and CPT. *In* Proceedings of the 2nd European Symposium on Penetration Testing, Amsterdam, 24-27.

Fargnoli, V., Gragnano, C.G., Boldini, D., and Amorosi, A. 2015a. 3D numerical modelling of soil-structure interaction during EPB tunnelling. Géotechnique, **65**(1): 23–27. https://doi.org/10.1680/geot.14.P.091.

Fargnoli, V., Boldini, D., and Amorosi, A. 2015b. Twin tunnel excavation in coarse grained soils: Observations and numerical back-predictions under free field conditions and in presence of a surface structure. Tunnelling and Underground Space Technology, **49**, 454-469. https://doi.org/10.1016/j.tust.2015.06.003.

Farrell, R., Mair, R., Sciotti, A., and Pigorini, A. 2014. Building response to tunnelling. Soils and foundations, **54**(3), 269-279. https://doi.org/10.1016/j.sandf.2014.04.003.

Formato, F. 2009. Analysis of the interaction between the excavation of metro line C in Rome and the Carducci school. M.Sc. thesis, Department of Structural and Geotechnical Engineering, Sapienza University of Rome, Italy (in Italian).

Franza, A., Marshall, A.M., Haji, T., Abdelatif, A.O., Carbonari, S., and Morici, M. 2017. A simplified elastic analysis of tunnel-piled structure interaction. Tunnelling and Underground Space Technology, **61**: 104–121. https://doi.org/10.1016/j.tust.2016.09.008.

Franzius, J.N., and Potts, D.M. 2005. Influence of mesh geometry on three-dimensional finite-element analysis of tunnel excavation. International Journal of Geomechanics, **5**(3): 256-266. https://doi.org/10.1061/(ASCE)1532-3641(2005)5:3(256).

Giardina, G., Hendriks, M.A.N., and Rots, J.G. 2010. Numerical analysis of tunnelling effects on masonry buildings: the influence of tunnel location on damage assessment. Advanced Material Research, **133**: 289–294.

Giardina, G., Hendriks, M.A.N., and Rots, J. G. 2015. Sensitivity study on tunnelling induced damage to a masonry façade. Engineering Structures, **89**, 111-129. https://doi.org/10.1016/j.engstruct.2015.01.042.

Kasper, T., and Meschke, G. 2004. A 3D finite element simulation model for TBM tunnelling in soft ground. International Journal for Numerical and Analytical Methods in Geomechanics, **28**(14): 1441-1460. https://doi.org/10.1002/nag.395.

Kavvadas, M., Litsas, D., Vazaios, I., and Fortsakis, P. 2017. Development of a 3D finite element model for shield EPB tunnelling. Tunnelling and Underground Space Technology, **65**: 22-34. https://doi.org/10.1016/j.tust.2017.02.001.

Lambrughi, A., Medina Rodríguez, L., and Castellanza, R. 2012. Development and validation of a 3D numerical model for TBM–EPB mechanized excavations. Computers and Geotechnics, **40**: 97-113. https://doi.org/10.1016/j.compgeo.2011.10.004.

Lee, K. M., and Rowe, R. K. 1991. An analysis of three-dimensional ground movements: the Thunder Bay tunnel. Canadian Geotechnical Journal, **28**(1): 25-41. https://doi.org/10.1139/t91-004.

Logarzo, A., Miliziano, S., Floria, V., and Pescara, M. 2011. Observed and predicted settlements induced by the construction of hydraulic tunnels in Buenos Aires. *In* Proceedings of the 7th International Symposium on Geotechnical Aspects of Underground Construction in Soft Ground, Rome, 2011. Balkema, Rotterdam, pp. 1011-1018.

Losacco, N., Burghignoli, A., and Callisto, L. 2014. Uncoupled evaluation of the structural damage induced by tunnelling. Géotechnique, **64**(8): 646–656. https://doi.org/10.1680/geot.13.P.213.

Maleki, M., Sereshteh, H., Mousivand, M., and Bayat, M. 2011. An equivalent beam model for the analysis of tunnel-building interaction. Tunnelling and Underground Space Technology, **26**(4), 524-533. https://doi.org/10.1016/j.tust.2011.02.006.

Mair, R. J., and Wood, D. M. 1987. Pressuremeter testing: Methods and interpretation. CIRIA Ground Engineering Report, Butterworths, London.

Mayne, P. W., and Kulhawy, F. H. 1982. K_0-OCR relationships in soil. Journal of the Soil Mechanics and Foundations Division, **108**(6): 851-872.

Mènard, L. 1976. Règles Relatives à l'Exécution des Essais Pressiométriques. Sols Soils, **7**(27).

Miliziano, S., Soccodato, F.M., and Burghignoli, A. 2002. Evaluation of damage in masonry buildings due to tunnelling in clayey soils. *In* Proceedings of the 3rd International Symposium on Geotechnical Aspects of Underground Construction in Soft Ground, Toulouse, 2002. Balkema, Rotterdam, pp. 335-340.

Moh, Z.C., and Hwang, R. N. 1996. Ground movements around tunnels in soft ground. *In* Proceedings of the International Symposium on Geotechnical Aspects of Underground Construction in Soft Ground, London, 1996. Balkema, Rotterdam, pp. 725-730.

Möller, S. C., and Vermeer, P. A. 2008. On numerical simulation of tunnel installation. Tunnelling and Underground Space Technology, **23**(4): 461-475. https://doi.org/10.1016/j.tust.2007.08.004.

Negro, A., and De Queiroz, P.I.B. 2000. Prediction and performance: a review of a numerical analyses for tunnels. *In* Proceedings of the International Symposium on Geotechnical Aspects of Underground Construction in Soft Ground, Tokyo 2000. Balkema, Rotterdam, pp. 409-418.

Ochmański, M., Modoni, G., and Bzówka, J. 2018. Automated numerical modelling for the control of EPB technology. Tunnelling and Underground Space Technology, **75**, 117-128. https://doi.org/10.1016/j.tust.2018.02.006.

Panet, M., and Guenot, A. 1982. Analysis of convergence behind the face of a tunnel. *In* Proceedings of the International Conference Tunnelling, Brighton, 1982. Institution of Mining and Metallurgy, London, pp. 197-204.

Peck, R.B. 1969. Deep excavations and tunnelling in soft ground. *In* Proceedings of the 7th International Conference on Soil Mechanics and Foundation Engineering, Mexico City, pp. 225-290.

Pickhaver, J.A., Burd, H.J., and Houlsby, G.T. 2010. An equivalent beam method to model masonry buildings in 3D finite element analysis. Computers & Structures, **88**(19-20): 1049–1063. doi:10.1016/j.compstruc.2010.05.006.

PLAXIS 3D Tunnel version 2.4. 2007. Finite Element Code for Soil and Rock Analyses. Plaxis, Delft.

Robertson, P. K., and Campanella, R. G. 1983. Interpretation of cone penetration tests. Part II: Clay. Canadian Geotechnical Journal, **20**(4): 734-745.

Rotisciani, G.M., and Miliziano, S. 2014. Guidelines for calibration and use of the Severn-Trent sand model in modeling cantilevered wall-supported excavations. International Journal of Geomechanics, **14**(6), 04014029. https://doi.org/10.1061/(ASCE)GM.1943-5622.0000373.

Rotisciani, G.M., Miliziano, S., and Sacconi, S. 2015. Design, construction and monitoring of a building with deep basements in Rome. Canadian Geotechnical Journal, **53**(2), 210-224. https://doi.org/10.1139/cgj-2015-0244.

Rowe, R.K., and Kack, G.J. 1983. A method of estimating surface settlement above tunnels constructed in soft ground. Canadian Geotechnical Journal, **20**(1): 11-22. https://doi.org/10.1139/t83-002.

Shah, R., A. Lavasan, A., Peila, D., Todaro, C., Luciani, A., and Schanz, T. 2018. Numerical study on backfilling the tail void using a two-component grout. Journal of Materials in Civil Engineering, **30**(3): 1-9.

Swoboda, G., and Abu-Krisha, A. 1999. Three-dimensional numerical modelling for TBM tunnelling in consolidated clay. Tunnelling and Underground Space Technology, **14**(3): 327-333. https://doi.org/10.1016/S0886-7798(99)00047-4.

Tamagnini, C., Miriano, C., Sellari, E., and Cipollone, N. 2005. Two-dimensional FE analysis of ground movements induced by shield tunnelling: the role of tunnel ovalization. Rivista Italiana di Geotecnica, **1**: 11-33.

Ventriglia, U. 2002. Geology of the City of Rome, Amministrazione Provinciale di Roma, Roma (in Italian).

Zhang, Z. X., Liu, C., Huang, X., Kwok, C. Y., and Teng, L. 2016. Three-dimensional finite-element analysis on ground responses during twin-tunnel construction using the URUP method. Tunnelling and Underground Space Technology, **58**: 133-146. https://doi.org/10.1016/j.tust.2016.05.001.

Zhou, H., Gao, Y., Zhang, C., Yang, F., Hu, M., Liu, H., and Jiang, Y. 2018. A 3D model of coupled hydro-mechanical simulation of double shield TBM excavation. Tunnelling and Underground Space Technology, **71**, 1-14. https://doi.org/10.1016/j.tust.2017.07.012.

Tables

Table 1. Physical and mechanical soil parameters.

Soil	Description	γ (kN/m^3)	c' (kPa)	φ' (°)	E (MPa)	E_0 (MPa)	K_0 -
R	coarse-grained soil	17.5	10	32	15-65	100-300	0.47
LSO	clayey silt and sandy silt	17.0	15	32	15-30	200-450	0.68
St/Ar	silty sand and clayey silt	20.0	10	35	25-80	300-600	0.64
Sg	sandy gravel	20.0	0	40	80-180	1000-1300	0.56

Table 2. Plate characteristics.

Plate	E (GPa)	ν -	EA (kN/m)	EI (kN·m^2/m)
TBM	210	0.3	$7.1 \cdot 10^7$	$6.8 \cdot 10^5$
Lining	38	0.2	$1.1 \cdot 10^7$	$8.6 \cdot 10^4$

Table 3. Hardening Soil parameters.

Soil	E_{50}^{ref} (MPa)	$E_{\mathrm{oed}}^{\mathrm{ref}}$ (MPa)	$E_{\mathrm{ur}}^{\mathrm{ref}}$ (MPa)	m (-)	p_{ref} (kPa)	R_{f} (-)
LSO	57	57	170	1.0	100	0.9
St/Ar	93	93	280	0.8	100	0.9

Table 4. Numerical analyses.

Analysis	Constitutive model	Stiffness (strain level)	Front pressure (kPa)	TBM conicity + overcut (mm)	Max. settlement (mm)
Class A prediction	MC*	Medium strains	150	20	7.8
Class A + actual pressure	MC	Medium strains	300	20	7.2
Updated class A	MC	Medium strains	300	30	9.6
E_0-analysis	MC	Small strains	300	30	5.9
HS-analysis	HS**	Non-linear	300	30	6.9
E_0 reduced conicity	MC	Small strains	300	20	4.9
HS reduced conicity	HS	Non-linear	300	20	5.0

* Elastic perfectly plastic with Mohr-Coulomb strength criterion; ** Hardening soil.

Figure captions

Fig. 1. Plan view of the building and the tunnels.

Fig. 2. Carducci school.

Fig. 3. Ground plan of the oldest part of the building.

Fig. 4. Geological map (adapted from Ventriglia, 2002).

Fig. 5. Geotechnical soil profile (section A-A of Fig. 1).

Fig. 6. Main soil mechanical properties and SPT tests results.

Fig. 7. Finite element mesh.

Fig. 8. Tunnelling simulation: (1) TBM shield; (2) front pressure; (3) shield conicity; (4) grout injection; (5) fresh grout; (6) hard grout; (7) lining.

Fig. 9. Building model.

Fig. 10. Preliminary analyses: numerical accuracy and computational effort for different mesh densities and tolerated errors (modified from Buselli et al., 2011).

Fig. 11. Preliminary analyses: greenfield volume loss along cross-section 2 during the advancement of tunnel B.

Fig. 12. Longitudinal settlements profiles at foundation level along section 1 during the advancement of tunnel B: comparison between greenfield and interaction analyses (adapted from Buselli et al., 2011).

Fig. 13. Settlements profile at foundation level at the end of tunnel B excavation along cross section 2: comparison between greenfield and interaction analyses and Gaussian curve.

Fig. 14. Earth pressure measurements inside the excavation chamber a) far away from and b) near to the Carducci school.

Fig. 15. Plan view of the monitoring system layout: mini-prisms on the buildings and landmarks on the road.

Fig. 16. Monitoring data: road settlements along section 11, tunnels advancements and earth pressures.

Fig. 17. Extrapolation of the settlements induced by the excavation of tunnel B only (benchmark 5B).

Fig. 18. Monitoring data: building settlements (mm).

Fig. 19. Comparison between greenfield numerical settlements and monitoring data at ground level: class A prediction update.

Fig. 20. Comparison between greenfield numerical settlements and monitoring data at ground level: influence of soil stiffness and soil constitutive model.

Fig. 21. Distributions of vertical deformations and vertical displacements above the tunnel crown at the end of the excavation.

Fig. 22. Evolution of the principal effective stresses in the transversal plane a) at springline depth and b) above the tunnel crown; c) vertical effective stress versus vertical strain at the crown.

Fig. 23. Comparison between greenfield numerical settlements and monitoring data at ground level: back-analyses.

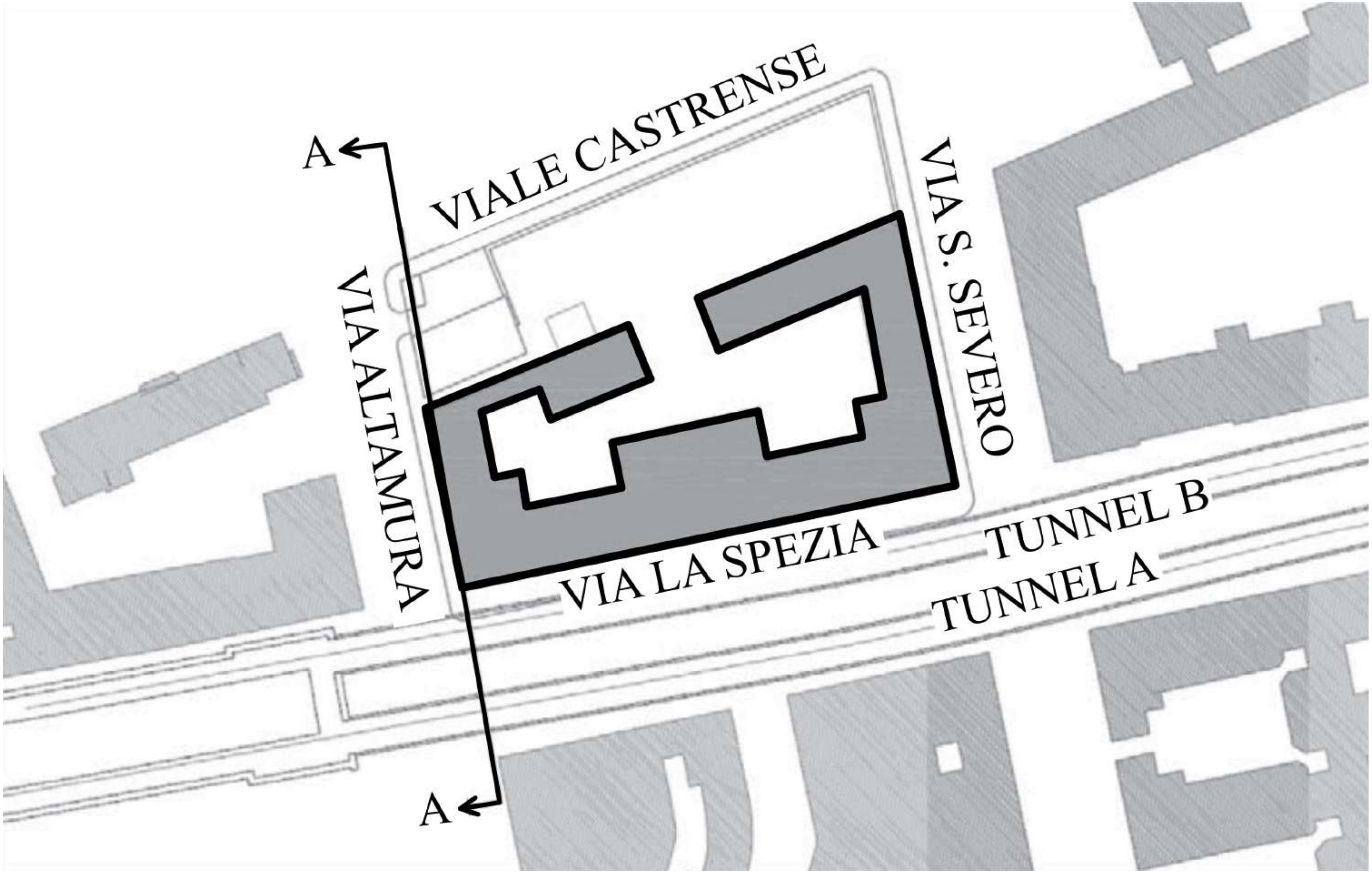
VIALE CASTRENSE
VIA S. SEVERO
VIA ALTAMURA
VIA LA SPEZIA
TUNNEL B
TUNNEL A
A
A


VIALE CASTRENSE
VIA S. SEVERO
VIA LA SPEZIA

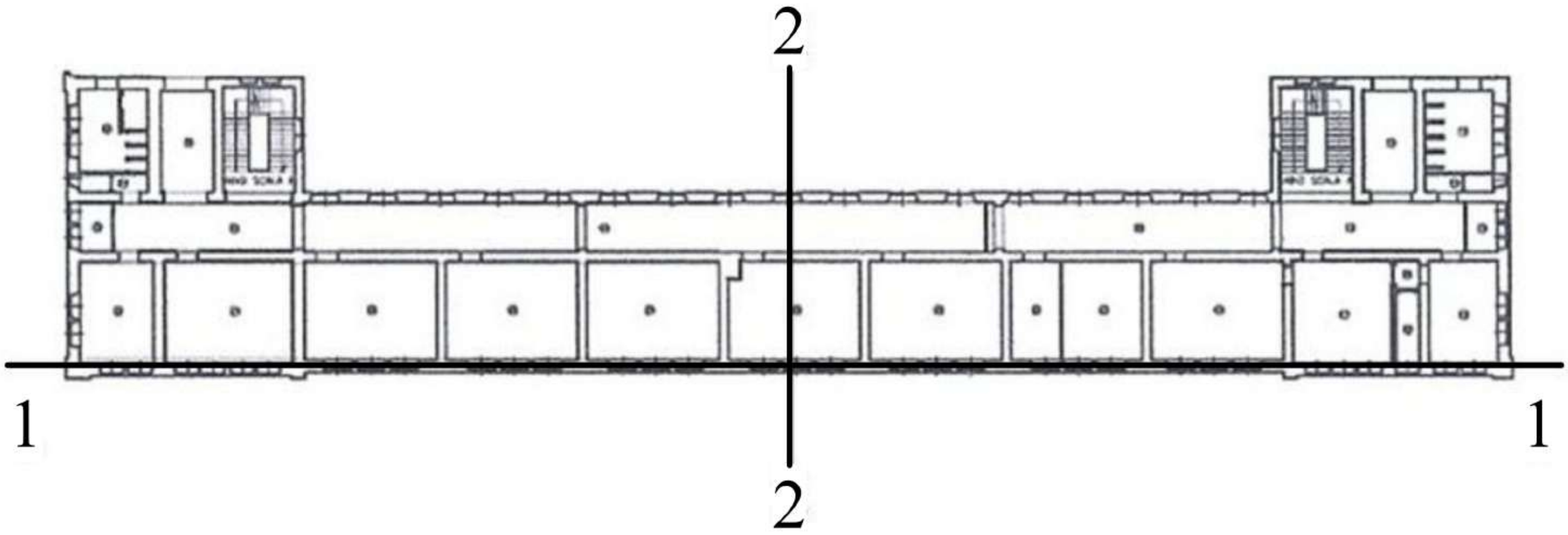
2
1
1
2

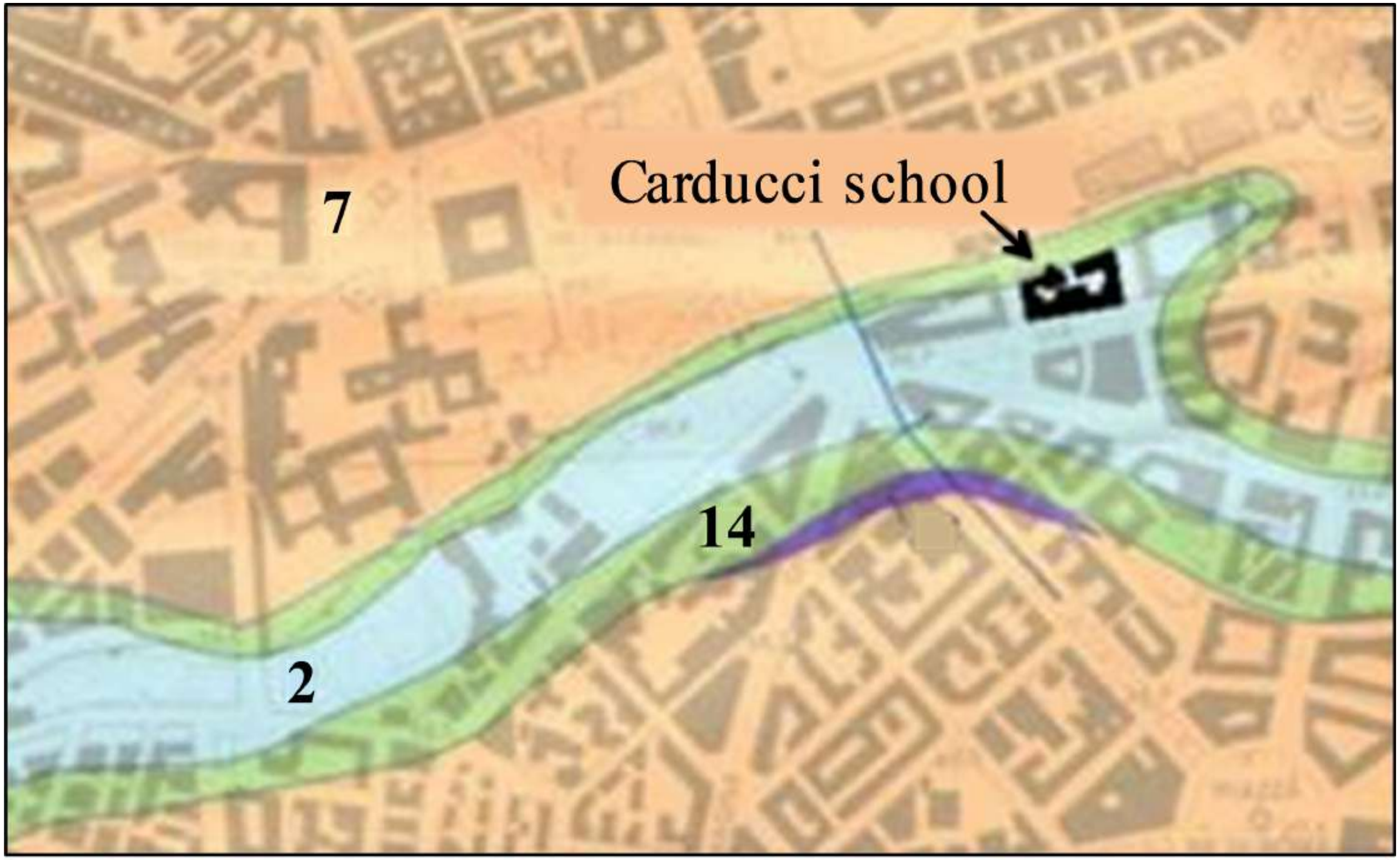

2	recent fluvial-alluvial deposit
7	pyroclastite
14	pre-volcanic fluvial deposit

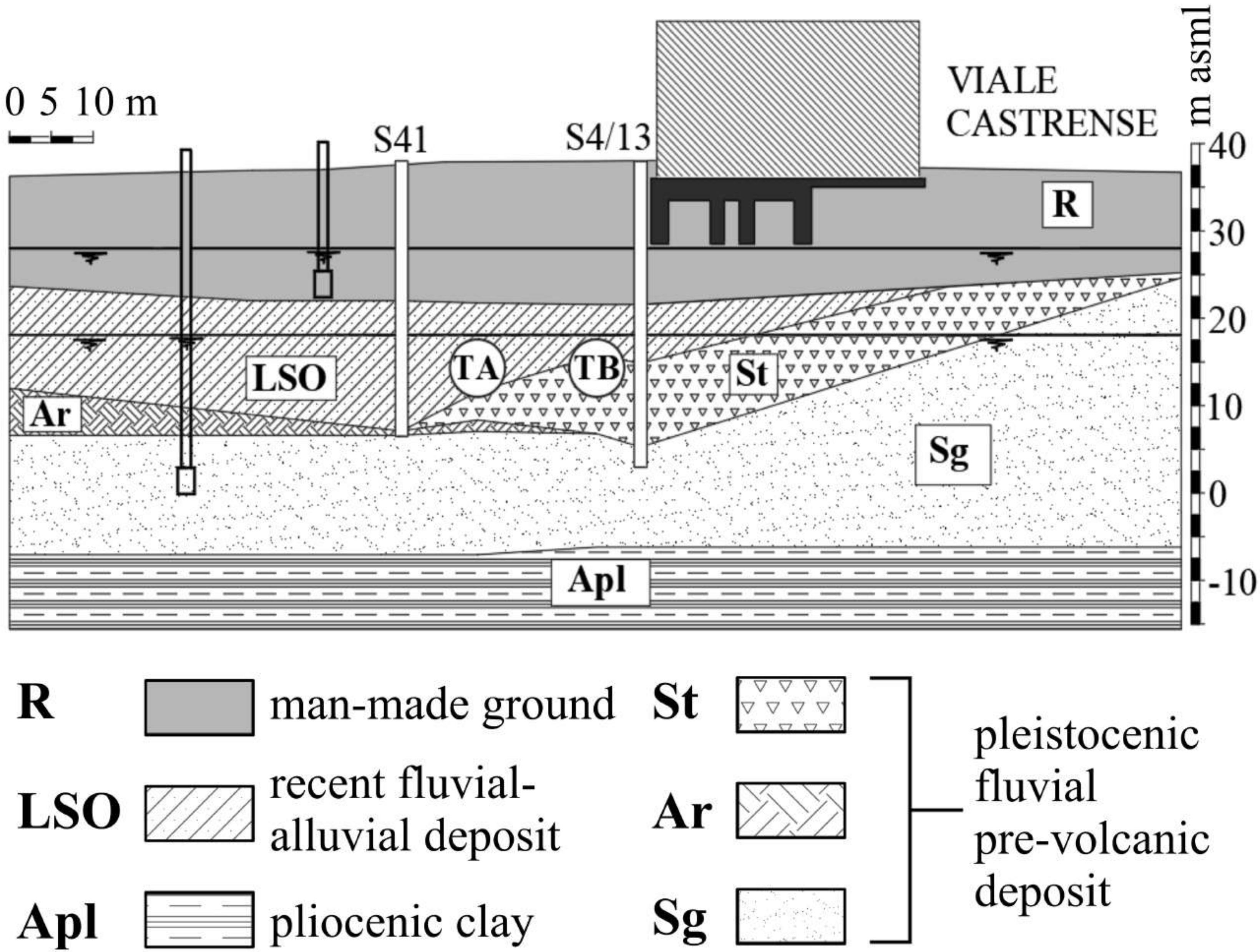
0 5 10 m
S41
S4/13
VIALE CASTRENSE
m asml
40
30
20
10
0
-10
R
LSO
Ar
TA
TB
St
Sg
Apl
R
man-made ground
LSO
recent fluvial-alluvial deposit
Apl
pliocenic clay
St
Ar
Sg
pleistocenic fluvial pre-volcanic deposit

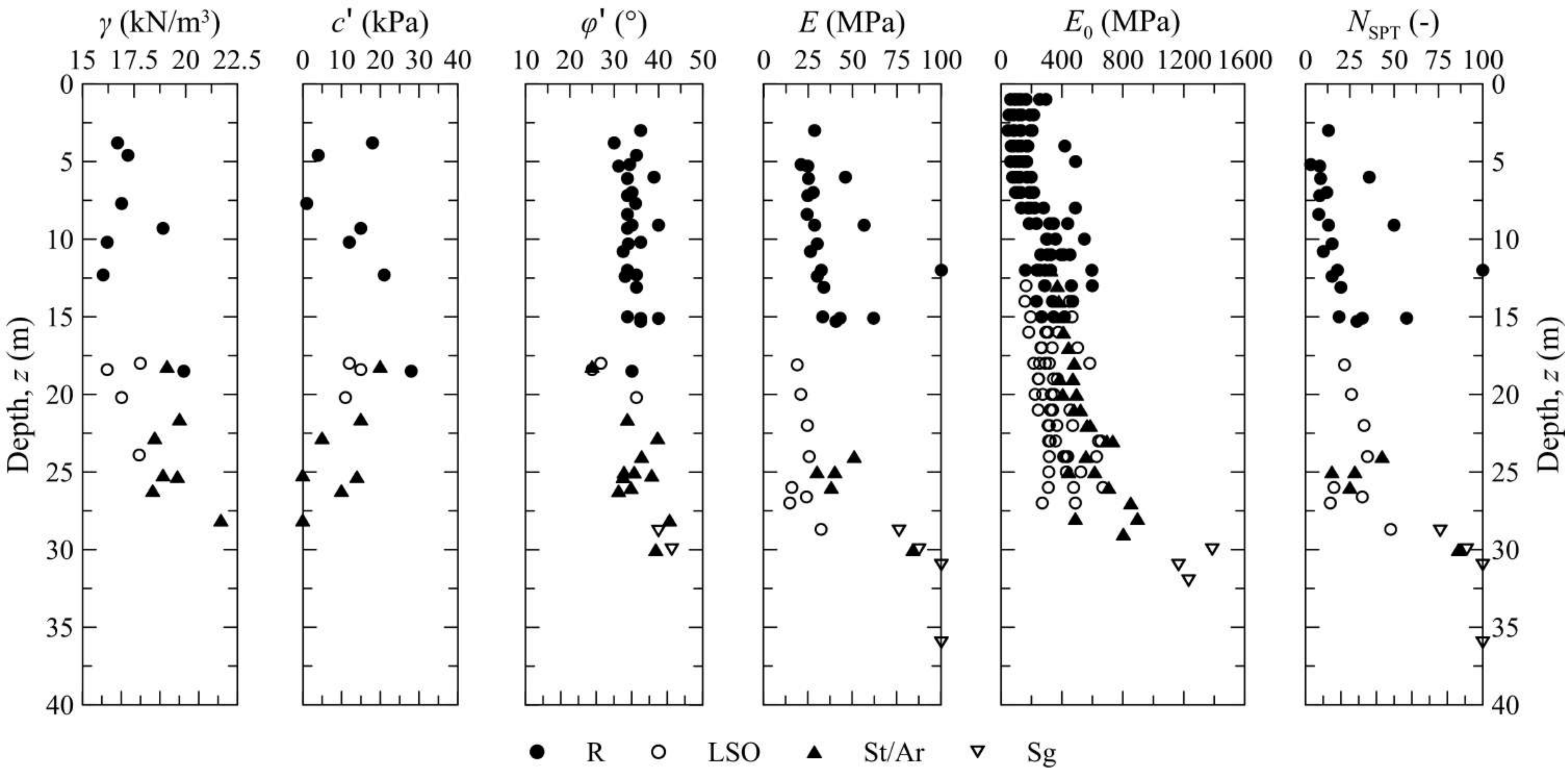

γ (kN/m³)
15 17.5 20 22.5
c' (kPa)
0 10 20 30 40
φ' (°)
10 20 30 40 50
E (MPa)
0 25 50 75 100
E0 (MPa)
0 400 800 1200 1600
NSPT (-)
0 25 50 75 100
Depth, z (m)
0 5 10 15 20 25 30 35 40
R
LSO
St/Ar
Sg

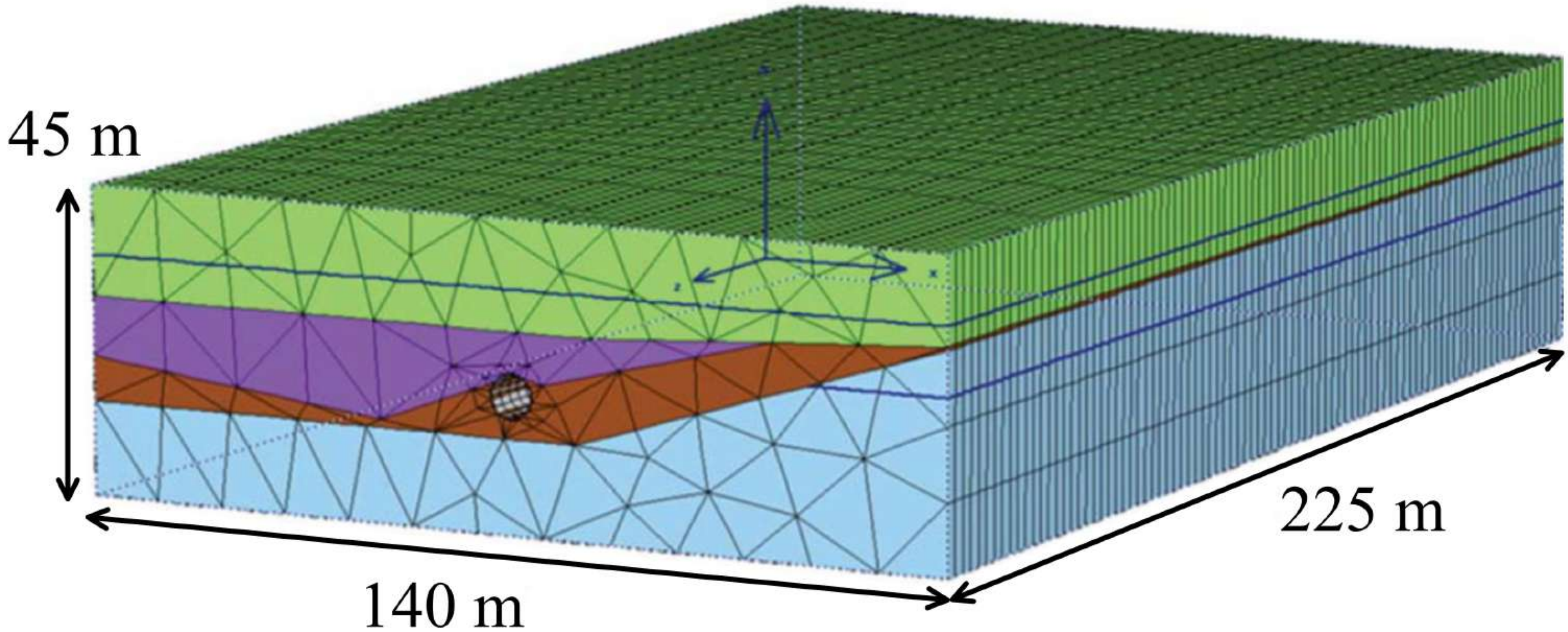
45 m
225 m
140 m

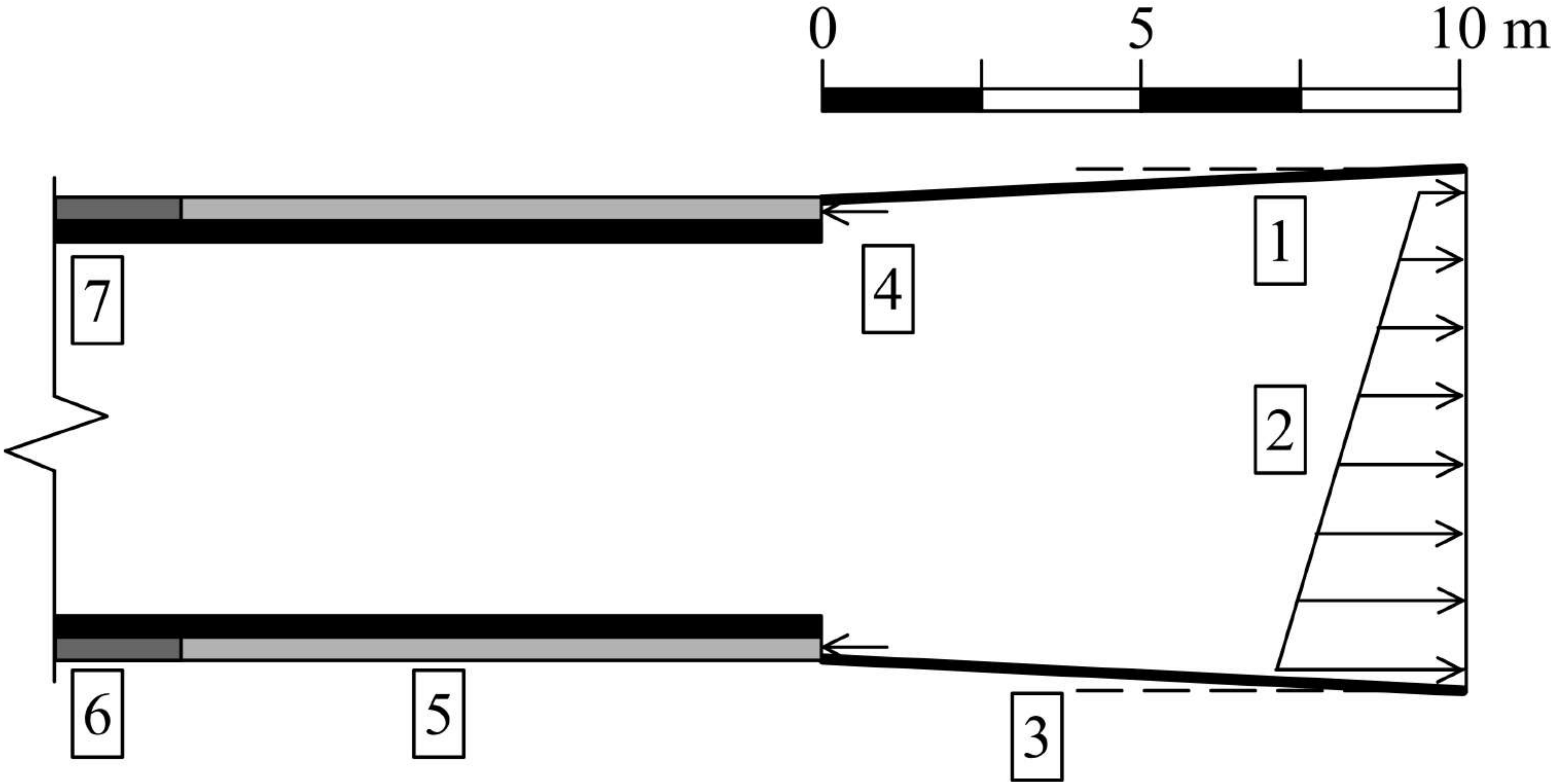

0
5
10 m
1
2
3
4
5
6
7

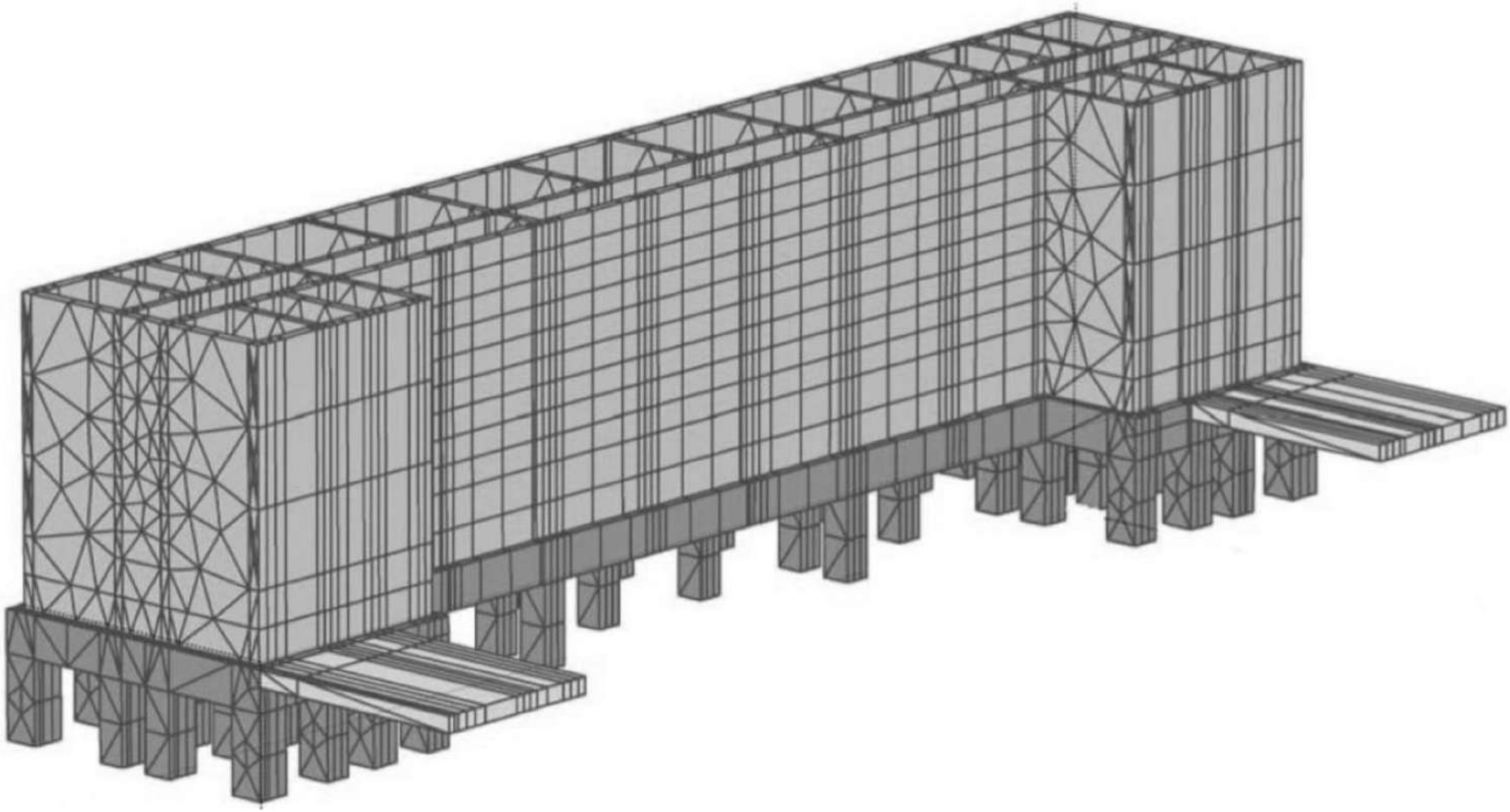

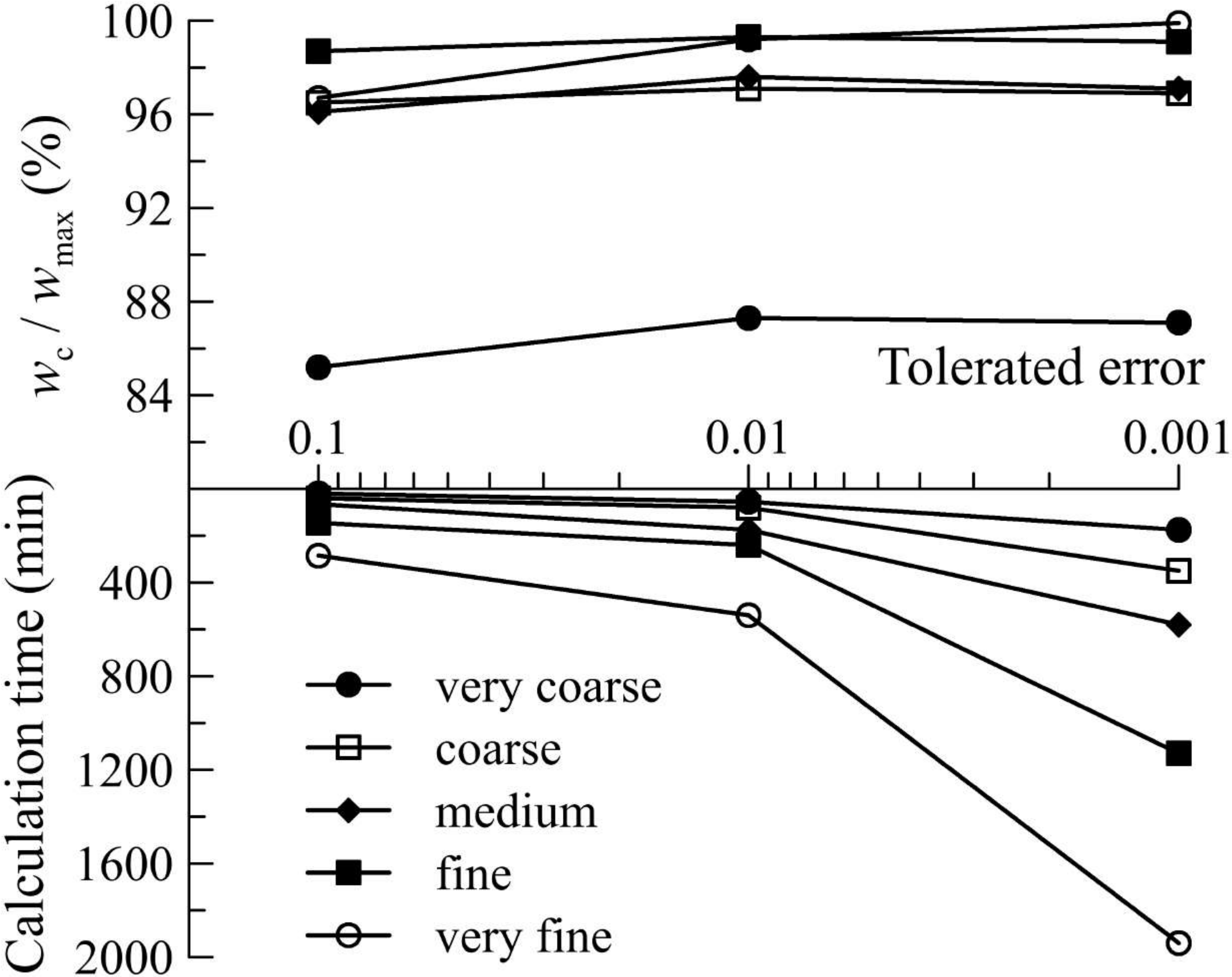

100
96
92
88
84
w_c / w_{max} (%)
Tolerated error
0.1
0.01
0.001
400
800
1200
1600
2000
Calculation time (min)
very coarse
coarse
medium
fine
very fine

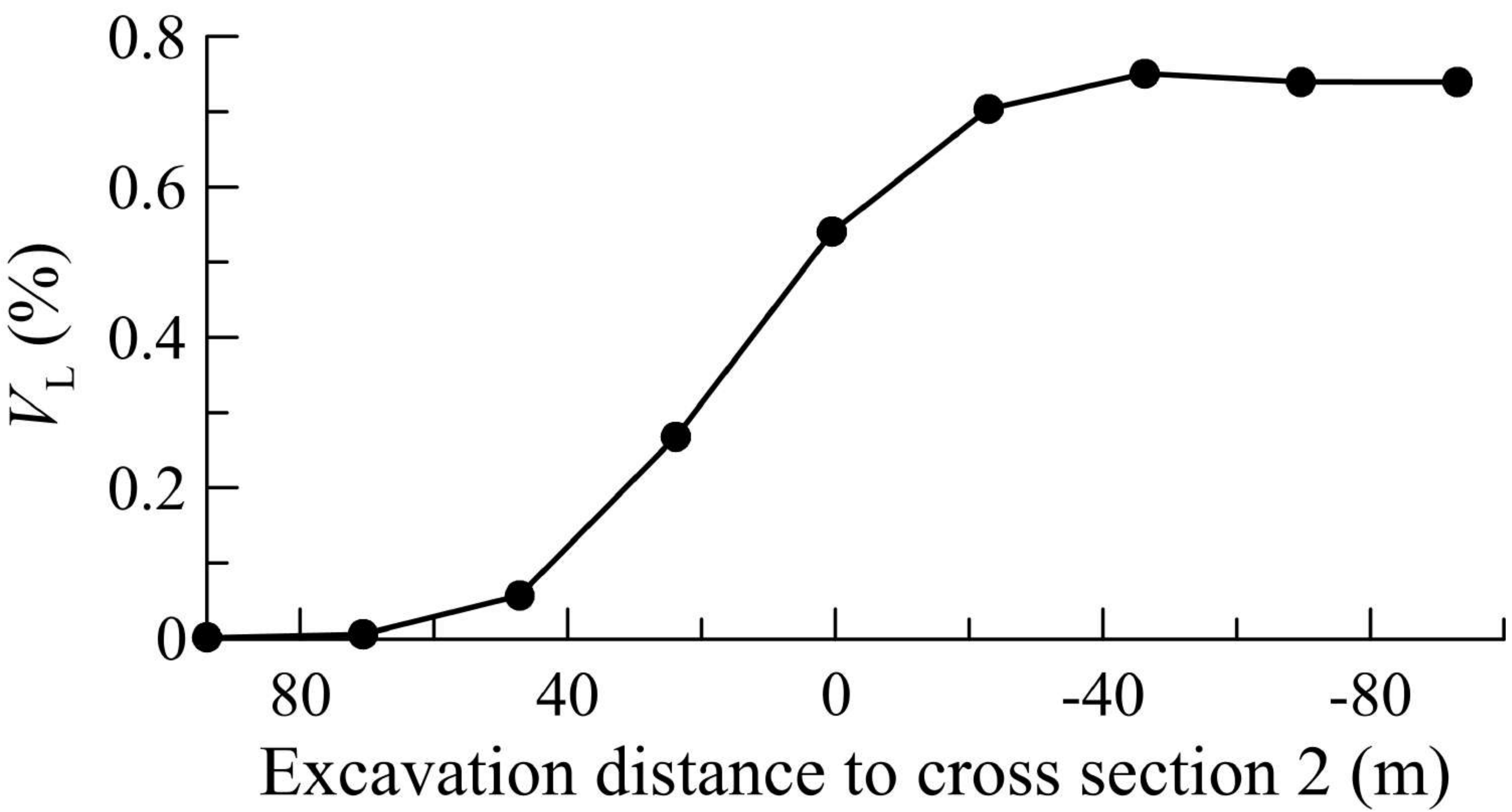

0.8
0.6
0.4
0.2
0
V_L (%)
80
40
0
-40
-80
Excavation distance to cross section 2 (m)

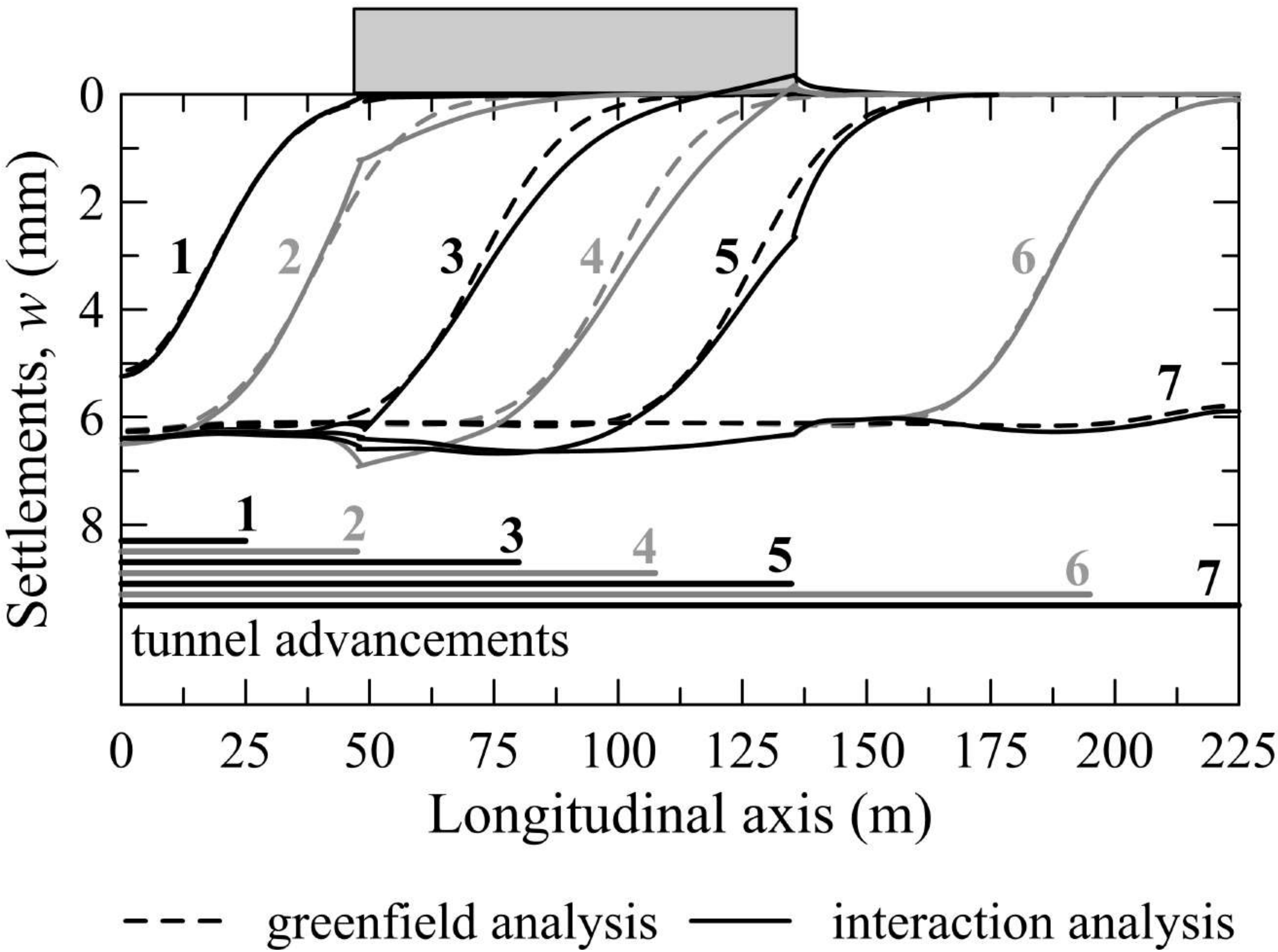

Settlements, w (mm)
0
2
4
6
8
1
2
3
4
5
6
7
tunnel advancements
0
25
50
75
100
125
150
175
200
225
Longitudinal axis (m)
greenfield analysis
interaction analysis

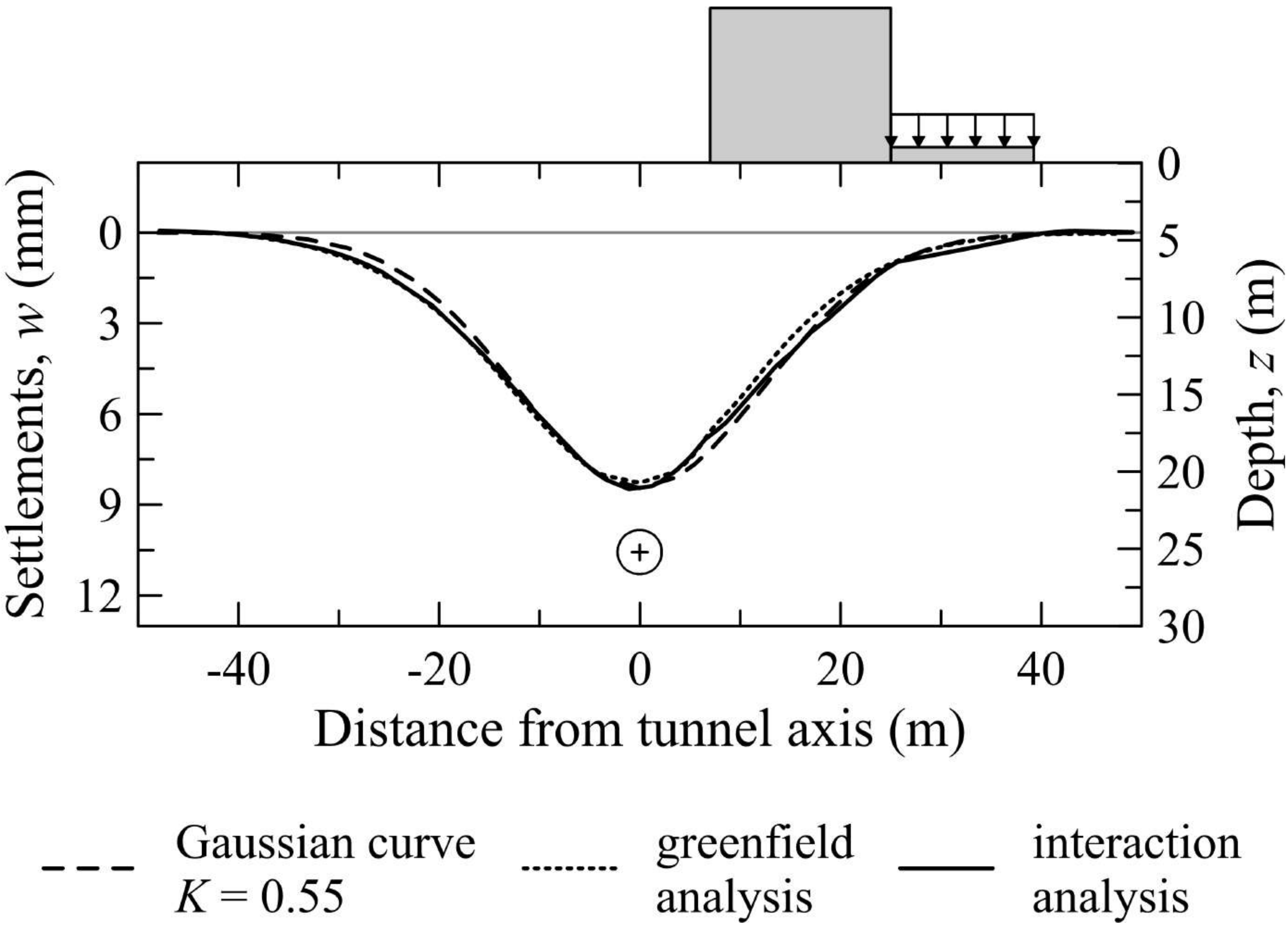

Settlements, w (mm)
0
3
6
9
12
Depth, z (m)
0
5
10
15
20
25
30
-40
-20
0
20
40
Distance from tunnel axis (m)
Gaussian curve
K = 0.55
greenfield
analysis
interaction
analysis

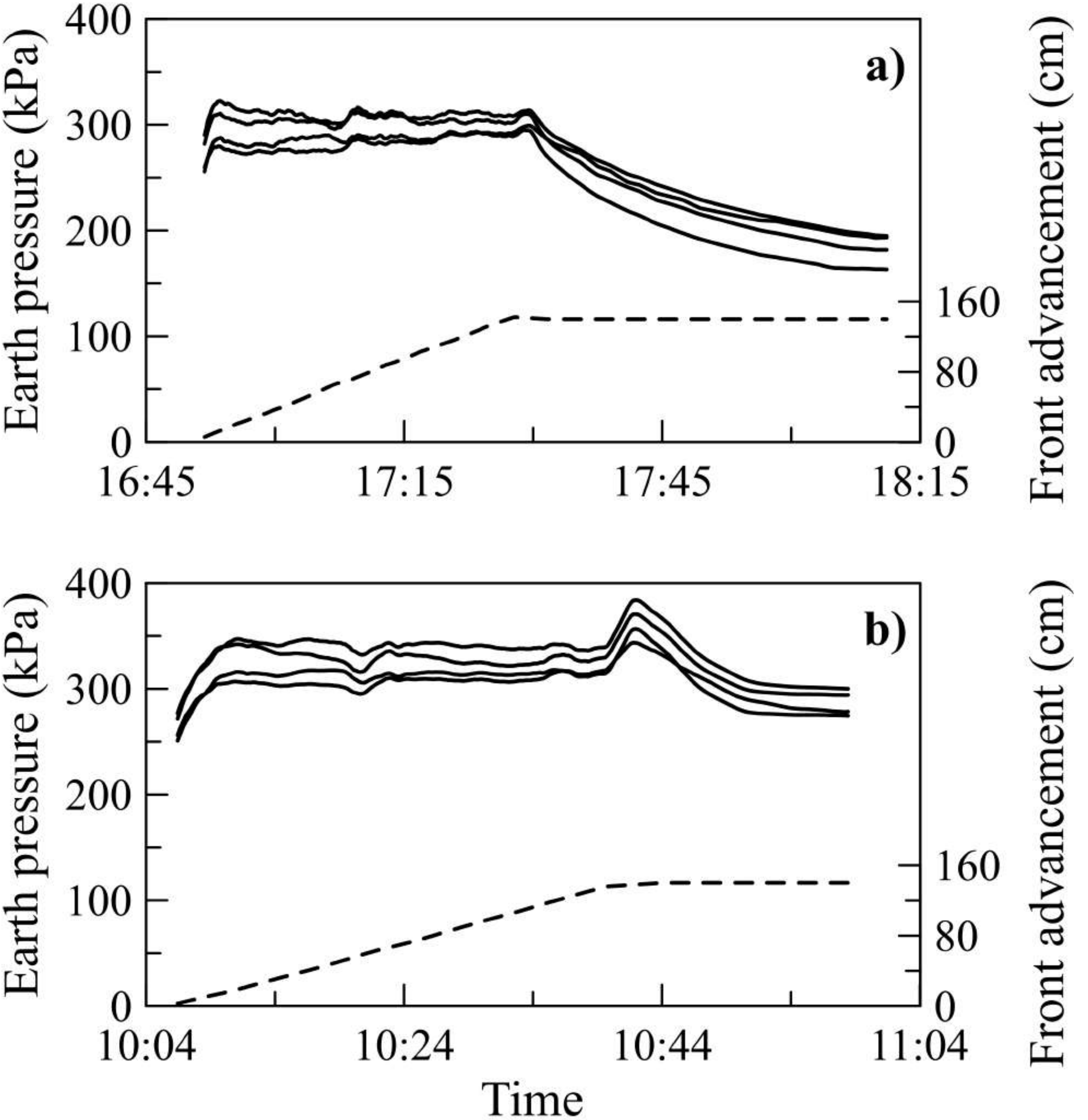
a)
Earth pressure (kPa)
Front advancement (cm)
400
300
200
100
0
160
80
0
16:45
17:15
17:45
18:15
b)
Earth pressure (kPa)
Front advancement (cm)
400
300
200
100
0
160
80
0
10:04
10:24
10:44
11:04
Time

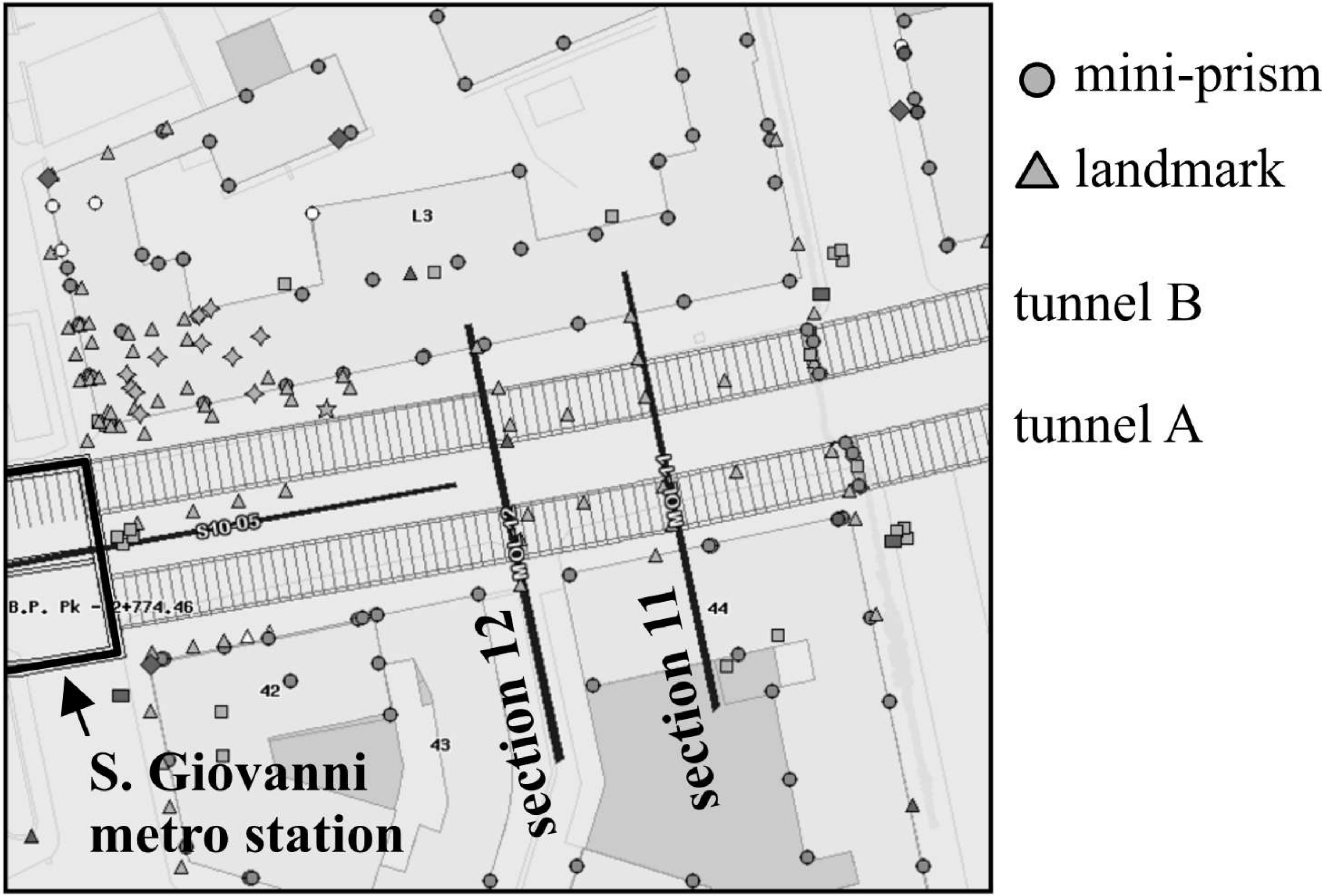
mini-prism
landmark
tunnel B
tunnel A
L3
S10-05
MOL-12
MOL-11
section 12
section 11
B.P. Pk
2+774.46
42
43
44
S. Giovanni
metro station

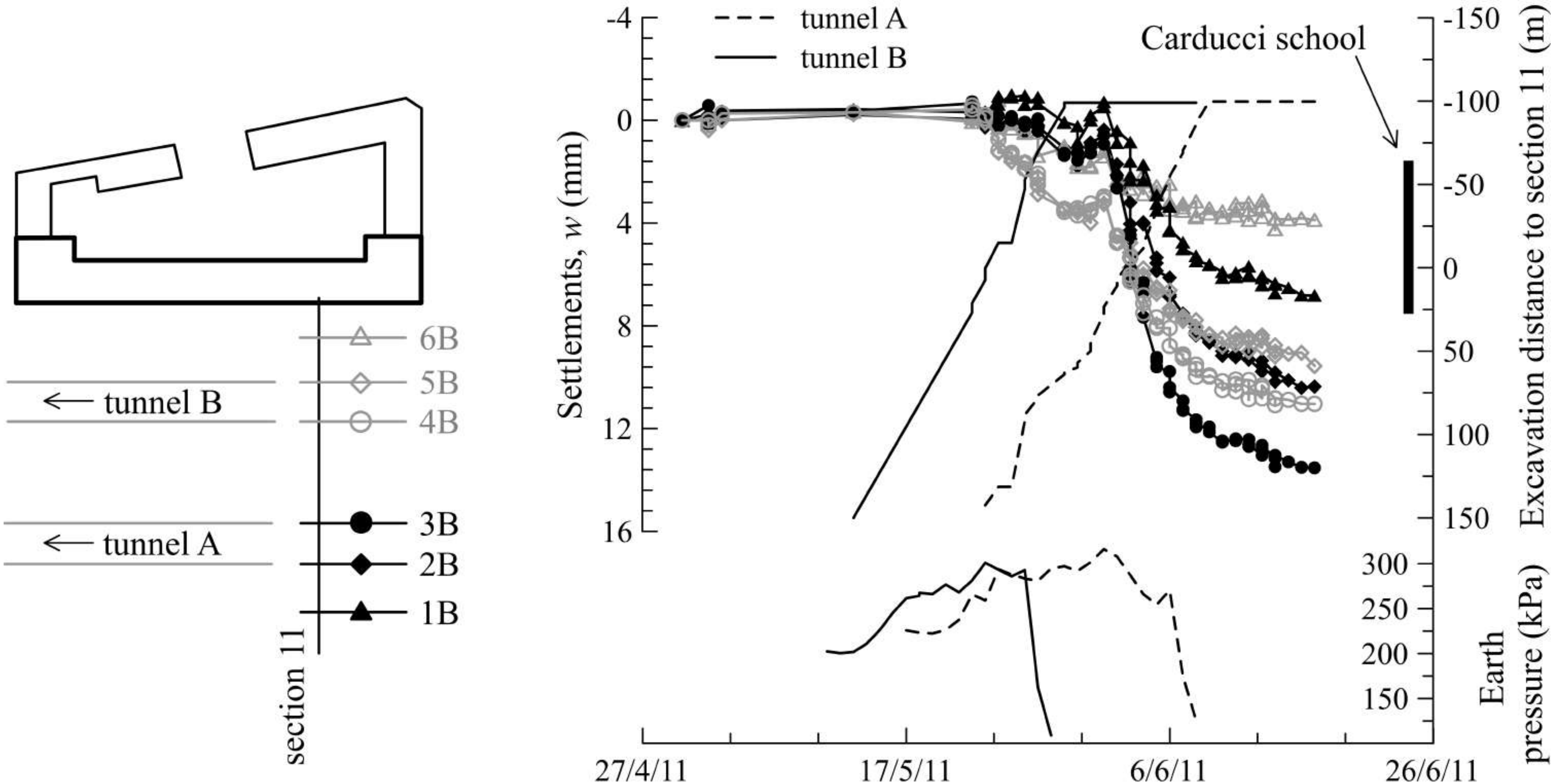

6B
5B
4B
tunnel B
3B
2B
1B
tunnel A
section 11
tunnel A
tunnel B
Carducci school
Settlements, w (mm)
-4
0
4
8
12
16
Excavation distance to section 11 (m)
-150
-100
-50
0
50
100
150
Earth pressure (kPa)
300
250
200
150
27/4/11
17/5/11
6/6/11
26/6/11

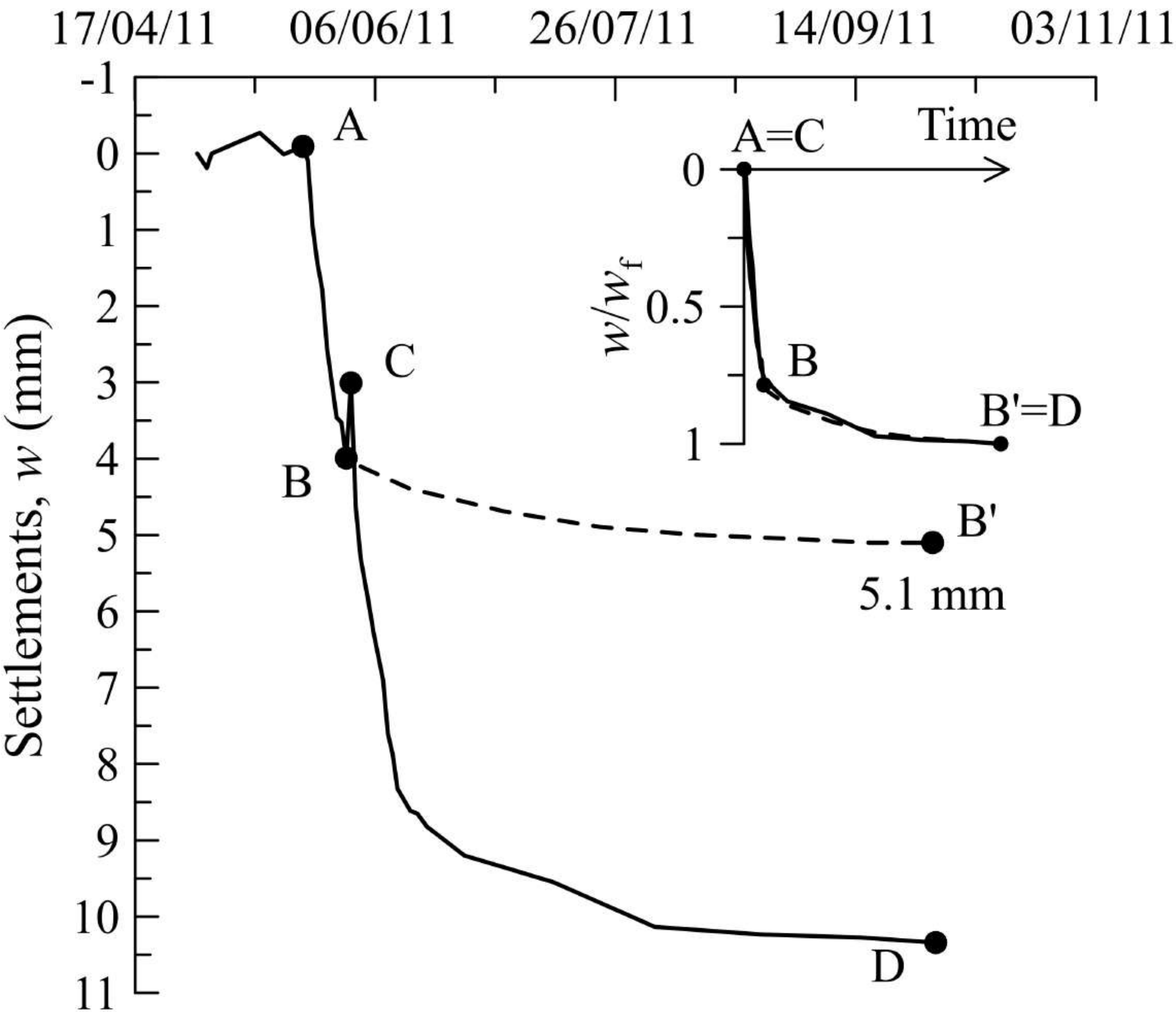
17/04/11
06/06/11
26/07/11
14/09/11
03/11/11
Settlements, w (mm)
-1
0
1
2
3
4
5
6
7
8
9
10
11
A
B
C
B'
5.1 mm
D
Time
A=C
B
B'=D
w/w_f
0
0.5
1

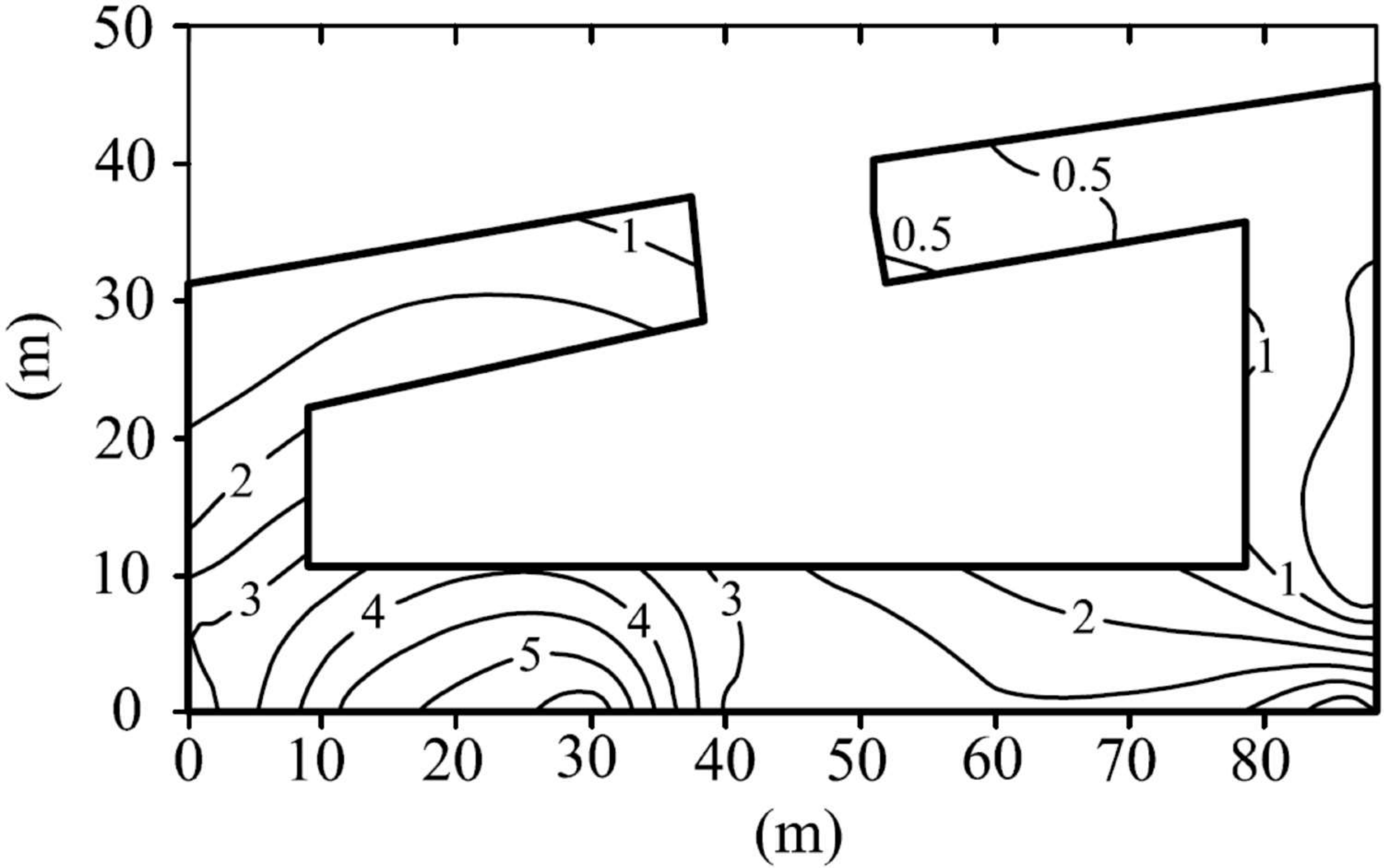

50
40
30
20
10
0
(m)
0
10
20
30
40
50
60
70
80
(m)
0.5
0.5
1
1
2
3
4
5
4
3
2
1

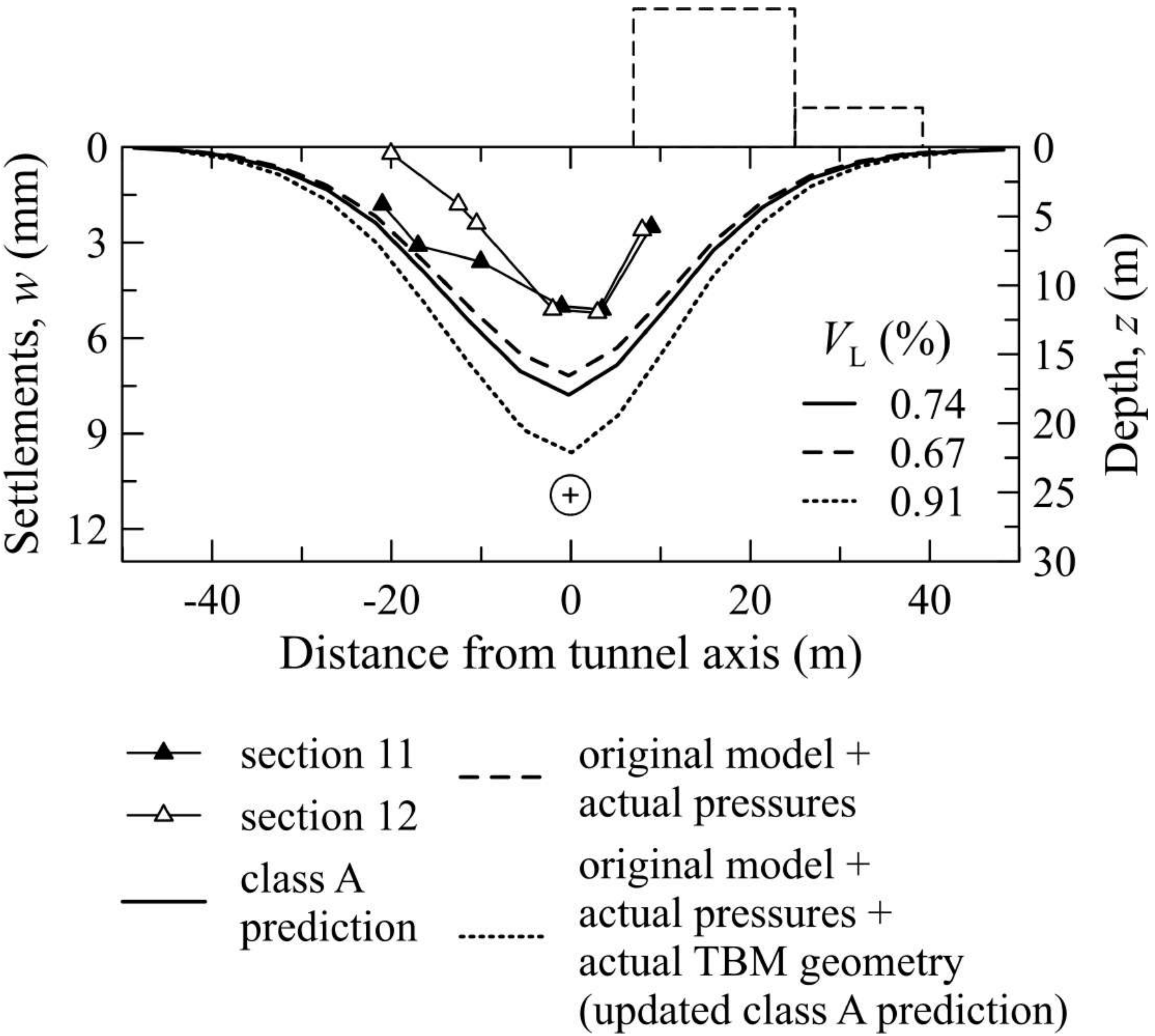

Settlements, w (mm)
0
3
6
9
12
Depth, z (m)
0
5
10
15
20
25
30
-40
-20
0
20
40
Distance from tunnel axis (m)
V_L (%)
0.74
0.67
0.91
section 11
section 12
class A prediction
original model + actual pressures
original model + actual pressures + actual TBM geometry (updated class A prediction)

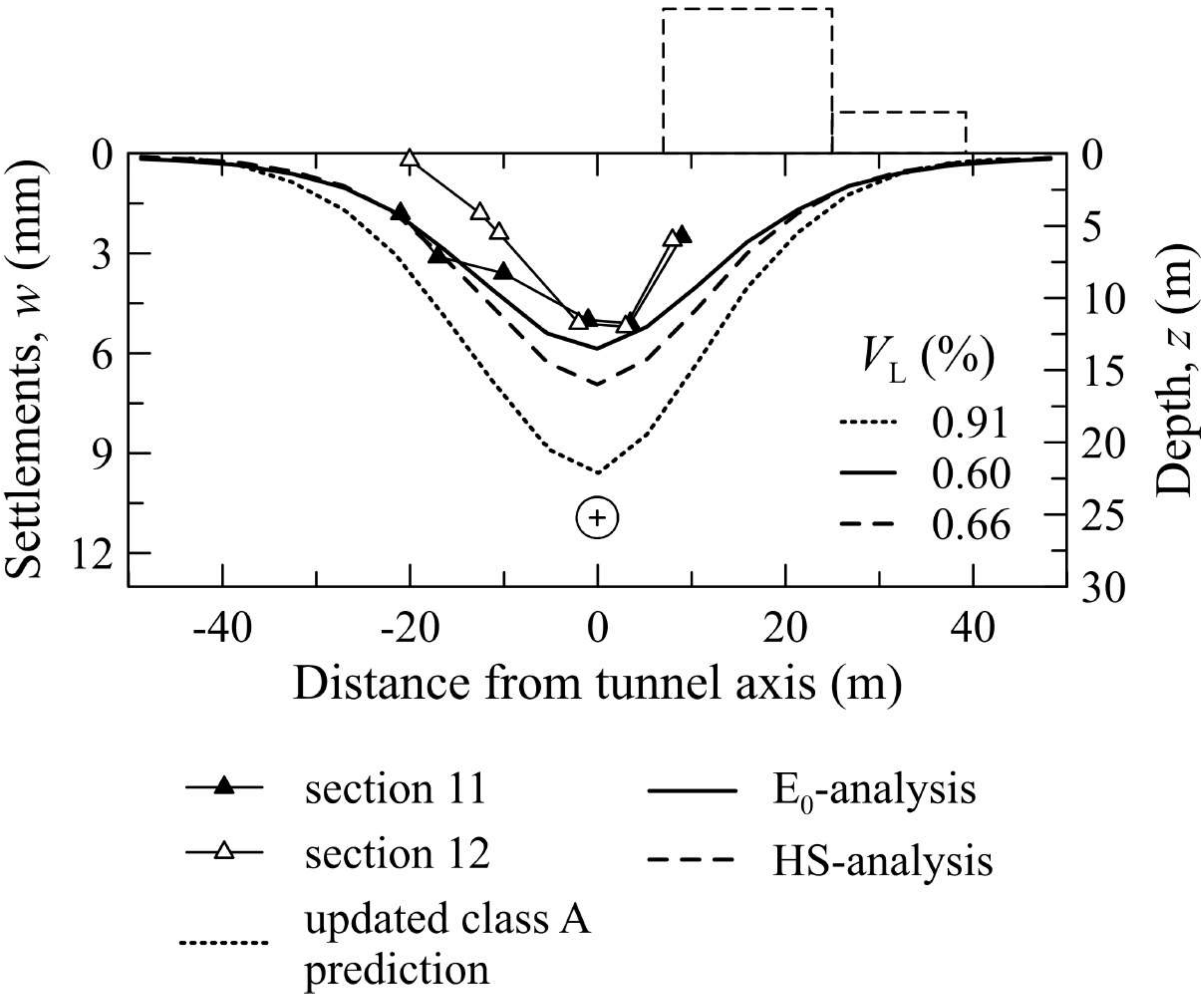

Settlements, w (mm)
0
3
6
9
12
Depth, z (m)
0
5
10
15
20
25
30
-40
-20
0
20
40
Distance from tunnel axis (m)
V_L (%)
0.91
0.60
0.66
section 11
section 12
updated class A prediction
E_0-analysis
HS-analysis

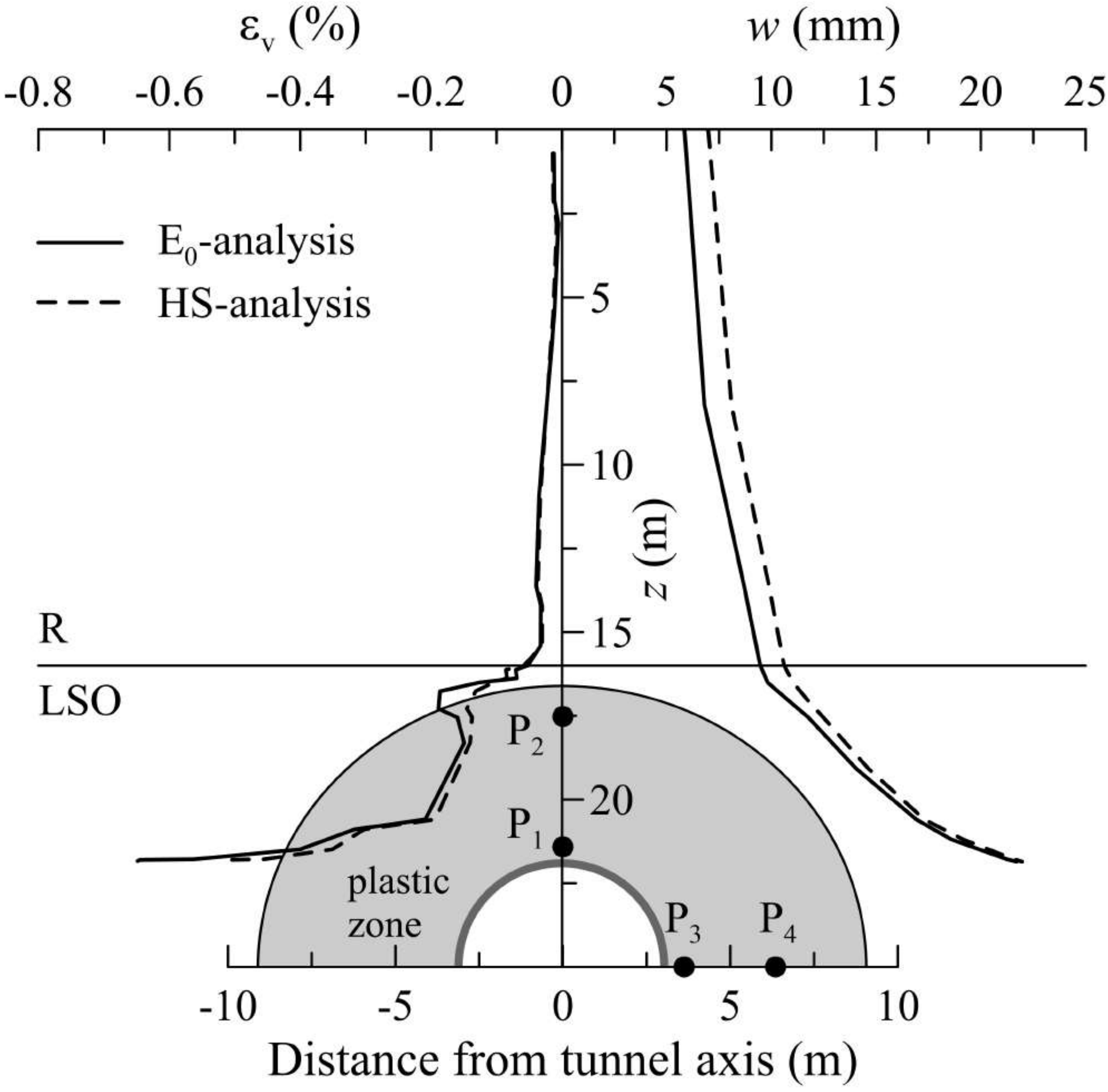

ε_v (%)
w (mm)
-0.8
-0.6
-0.4
-0.2
0
0
5
10
15
20
25
E_0-analysis
HS-analysis
5
10
z (m)
15
20
R
LSO
P_2
P_1
P_3
P_4
plastic zone
-10
-5
0
5
10
Distance from tunnel axis (m)

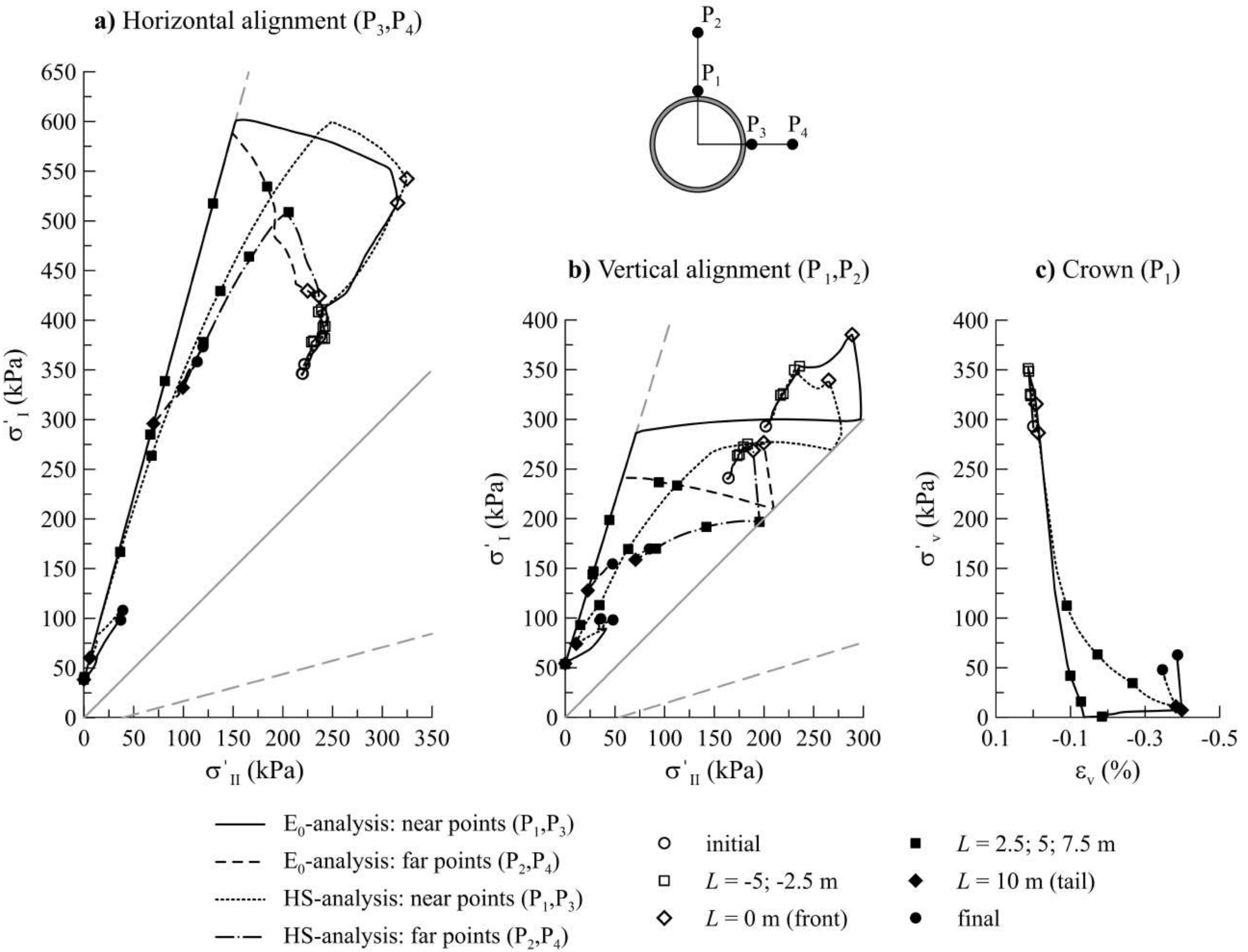

a) Horizontal alignment (P3,P4)
b) Vertical alignment (P1,P2)
c) Crown (P1)
P1
P2
P3
P4
σ'I (kPa)
σ'II (kPa)
σ'v (kPa)
εv (%)
E0-analysis: near points (P1,P3)
E0-analysis: far points (P2,P4)
HS-analysis: near points (P1,P3)
HS-analysis: far points (P2,P4)
initial
L = -5; -2.5 m
L = 0 m (front)
L = 2.5; 5; 7.5 m
L = 10 m (tail)
final

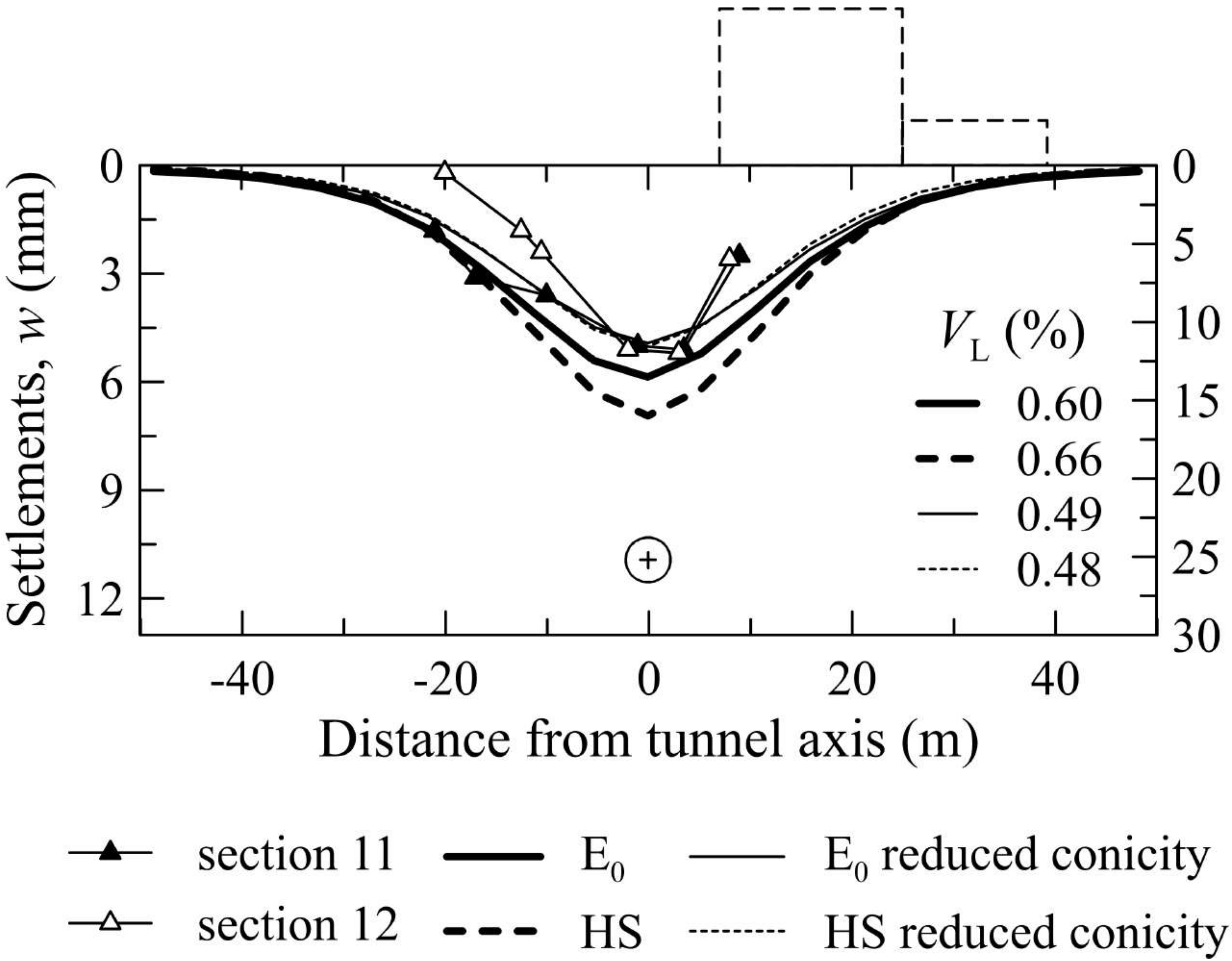

Settlements, w (mm)
0
3
6
9
12
Depth, z (m)
0
5
10
15
20
25
30
-40
-20
0
20
40
Distance from tunnel axis (m)
V_L (%)
0.60
0.66
0.49
0.48
section 11
section 12
E_0
HS
E_0 reduced conicity
HS reduced conicity